

Geochemistry, Geophysics, Geosystems

RESEARCH ARTICLE

10.1029/2020GC009076

Key Points:

- Terror Rift east margin geometry has 4 segments that alternate from fault controlled to dip controlled
- Late Oligocene shift from orthogonal to oblique rifting or transtensional strike-slip
- Fault activity continued after Miocene time, with sea floor scarps

Supporting Information:

- Supporting Information S1

Correspondence to:

C. Sauli,
csauli@inogs.it

Citation:

Sauli, C., Sorlien, C., Busetti, M., De Santis, L., Geletti, R., Wardell, N., & Luyendyk, B. P. (2021). Neogene development of the Terror Rift, western Ross Sea, Antarctica. *Geochemistry, Geophysics, Geosystems*, 22, e2020GC009076. <https://doi.org/10.1029/2020GC009076>

Received 6 APR 2020

Accepted 5 JAN 2021

Neogene Development of the Terror Rift, Western Ross Sea, Antarctica

C. Sauli¹ , C. Sorlien² , M. Busetti¹ , L. De Santis¹ , R. Geletti¹ , N. Wardell¹ , and B. P. Luyendyk² 

¹National Institute of Oceanography and Applied Geophysics-OGS, Trieste, Italy, ²Earth Research Institute, University of California, Santa Barbara, CA, USA

Abstract The Terror Rift is a 350 km-long, 50–70 km-wide, north-trending deep basin in the western Ross Sea, adjacent to the Transantarctic Mountains. The Terror Rift lies within the broader Victoria Land Basin, which experienced 100 km of a mid-Cenozoic extension. New fault and post-29 Ma seismic stratigraphic interpretations were developed using all the seismic reflection data available from the Antarctic Seismic Data Library System and were correlated to all the scientific coreholes. A new 3D velocity model was used for depth conversions. Depth-converted seismic profiles are used to image the faulting along the rift margins. Two segments of steep normal-separation faults, which are connected by a broad anticline, border the eastern margin, whereas steep to sub vertical faults, combined with a stratal dip, produce the relief present at the western margin. The overall geometry of the Terror Rift shows an asymmetric half-graben structure with a main bounding fault that dips alternatively eastward and westward in the southern and in the central parts, until it becomes a symmetric graben in the north. Both the eastern and western faults were active since at least 29 Ma in the southern and central Terror Rift and at least since 21 Ma in the north. This fault activity appears to have continued within the whole Terror Rift into post-Miocene time, as suggested by the significant component of post-Miocene vertical slip. The measurements of large sedimentary rock thicknesses changes over time between the rift shoulders and the deepest part of the basin and agree with the continuous faulting and relative subsidence in the southern Terror Rift that occurred between 29 and 13 Ma. These changes differ from several published papers that proposed that no significant tectonic activity occurred between 23 and 13 Ma. Despite the growth of the Terror Rift basin, the extension after 21 Ma was only ~2–4 km across offshore mapped faults in the Terror Rift, and this minor extension agrees with a published plate tectonic study that suggests that the Terror Rift was a transtensional dextral transform boundary between 26 and 11 Ma. Therefore, the Terror Rift may have changed from an orthogonal rift into a transtensional transform boundary after 26 Ma, with the faulting after 11 Ma considered to be intraplate deformation.

1. Introduction

The Terror Rift, which is located in the southwestern sector of the Ross Sea (Antarctica), is a narrow and deep basin that extends for 350 km, between Ross Island and Cape Washington, within the broader Victoria Land Basin (VLB; Figure 1). The Terror Rift is ~75 km-wide and includes the 25–35 km-wide faulted Discovery Graben; it is flanked on the eastern side by the 25–40 km-wide volcanically intruded Lee Arch (Cooper et al., 1987a). Southward continuation of the Terror Rift for an additional 300 km beneath the Ross Ice Shelf is suggested by airborne gravity and magnetic data (Tankersley et al., 2018). Inversion of the gravity data reveals a deep, narrow sedimentary basin, with a left stepover (jog to the east looking south) near Ross Island (Jordan et al., 2020; Tinto et al., 2019).

The Terror Rift is one of the youngest parts of the West Antarctic Rift System (WARS), which is a Mesozoic-Cenozoic continental rift system that extends along a strike for 3,200 km from the Weddell Sea to the Ross Sea. The WARS extensional area includes the crustal block assemblage of West Antarctica and the rift shoulder on the border of the East Antarctic craton. During the Late Cretaceous and Paleogene WARS phases within the Ross Sea, part of the Ross Embayment, the E-W stretching of continental crust resulted in several hundred kilometers of extension (e.g., D. S. Wilson & Luyendyk, 2009). The subsidence related to this crustal thinning produced four main broad N-S basins (e.g., Victoria Land Basin, connected to Northern

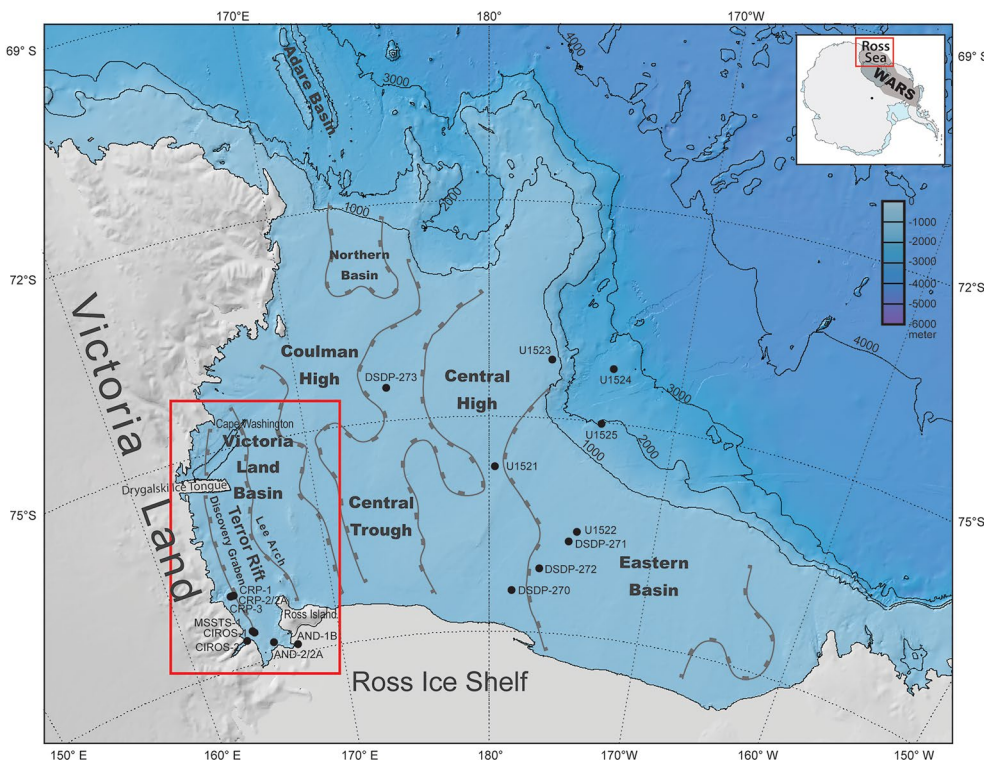


Figure 1. Ross Sea bathymetric map with the main structural highs and basins outlined in gray and the drillhole positions shown (contours every 1,000 m). The red box in the inset map displays the location of this figure, and the red rectangle in the figure locates the study area of the Terror Rift in the western Ross Sea, as observed in Figures 2 and 5. The inset map shows the location of the West Antarctic Rift System (WARS). The DEM model was constructed with GeoMapApp (www.geomapapp.org; CC by Ryan et al., 2009).

Basin; Central Trough; and Eastern Basin) (Brancolini et al., 1995b; F. J. Davey & Brancolini, 1995; F. J. Davey et al., 1982; Figure 1).

The timing of the extension differs among basins within the Ross Sea part of the WARS. Extension occurred between 105 Ma and 80 Ma in the eastern Ross Sea (P. G. Fitzgerald & Baldwin, 1997; Lawver & Gahagan, 1994; Luyendyk et al., 1996; Siddoway et al., 2004). Sea floor spreading across what is now a deep bathymetric basin, which is aligned with the sedimentary basin Central Trough, has been proposed for ~80–55 Ma (Cande & Stock, 2006; D. S. Wilson & Luyendyk, 2009). This sea floor spreading is linked to the extension and crustal thinning in the Central Trough and in the Northern Basin. Sea floor spreading of about 180 km occurred across the Adare Trough between 43 and 26 Ma; this spreading affected the area that is now filled with sediments in the Northern Basin (Cande et al., 2000; Cande & Stock, 2006; Davey et al., 2006, 2016; Granot et al., 2010, 2013). The Victoria Land Basin formed at the same time, and it was stretched to 95–100 km of its total 140–160 km width (Cande & Stock, 2006; F. J. Davey & De Santis, 2006). The Terror Rift is considered to be as a younger feature that formed during the Neogene inside the already existing Victoria Land Basin (Cooper et al., 1987a, 1987b; F. J. Davey & Brancolini, 1995; C. R. Fielding et al., 2006, 2008; Henrys et al., 2007), with an initial E-W orthogonal crustal extension, across N-S faults (Cooper et al., 1987a; Hall et al., 2007).

The timing of the initiation of the focused extension and subsidence of the Terror Rift within the Victoria Land Basin is an open question, with two sets of conflicting interpretations and models. The first set of models proposes that the Terror Rift extension and tectonic subsidence started during the Middle Miocene time after a period of inactivity and passive thermal subsidence between 23 and 13 Ma (R. C. Fielding, 2018; Fielding et al., 2008; Hall et al., 2007; Henrys et al., 2007). These models are based on examinations of the Cape Roberts and ANDRILL cores and on interpretations of seismic reflection data (R. C. Fielding, 2018;

Fielding et al., 2008; Henrys et al., 2007). The other model proposes that tectonic motion across the western Ross Sea was continuous between 43 Ma and 11 Ma, with a change in the relative motion direction at 26 Ma (Cande et al., 2000; Granot & Dymant, 2018; Granot et al., 2013). This model is based on plate tectonic reconstructions that used marine magnetic anomalies and fracture zone orientations preserved in the deep ocean, including the Adare Trough. The calculated pole of rotation between East and West Antarctica from 26 to 11 Ma resulted in a total right-lateral displacement of 30 km across Terror Rift, and includes between 0 and 20 km of extension (Granot & Dymant, 2018).

Oblique rifting initiated from 50 to 40 Ma has been proposed for the westernmost Ross Sea and the adjacent Transantarctic Mountains, based on geological field work and incorporating the timing of denudation (Rossetti et al., 2006; Storti et al., 2008; T. J. Wilson, 1995). Alternatively, a mid-Cenozoic (~30 Ma) change from the Paleogene E-W extension to Neogene oblique rifting, including strike-slip faulting, was interpreted (Hamilton et al., 2001; Salvini & Storti, 1999; Salvini et al., 1997). The Neogene oblique rifting hypotheses are based in part on interpretation of seismic reflection data that were correlated with scientific core holes. The Salvini et al. (1997) model proposed that long NW-SE right-lateral faults to cut from North Victoria Land (Figure 1) across the Northern Basin and Adare Trough to the central and eastern Ross Sea. This model was disproved by additional newer seismic reflection data, and by the lack of offsets in the N-S oriented marine magnetic anomalies, some of which are continuous between the Adare Trough and Northern Basin (F. J. Davey et al., 2016; Granot et al., 2010).

We present a comprehensive study of the geometry of Terror Rift in the Ross Sea, and its evolution through late Cenozoic time. This study is based on interpretations of faults and of stratigraphy as imaged on all the available seismic reflection data and sampled by scientific core holes. The rift is studied in detail over its full 350 km length north of the ice shelf edge. We outline the Terror Rift geographically as the deep sedimentary basin that formed in the western part of the Victoria Land Basin, and temporally by post-dating the de-activation of the eastern Victoria Land Basin rifting, which occurred sometime before the formation of a 26–30+ Ma unconformity (RSU6, Figure 3).

2. Data Set and Methods

This study utilized seismic reflection data, bathymetry, and stratigraphic data from deep scientific core drilling (Figure 2). The seismic reflection data set includes all the multichannel seismic reflection data (MCS) available from the SCAR Antarctic Seismic Data Library System for Cooperative Research (<https://sdls.ogs.trieste.it/>; Childs et al., 1994) for the study area. In addition, the following single channel seismic reflection profiles (SCS) were integrated: Italian data acquired in 2001/2002 (Sauli et al., 2014) and United States of America data collected in 1990 (Anderson & Bartek, 1992; Bartek et al., 1996) and 2003 (Bart, 2004). The water is deep enough over much of the study area that the SCS images the mapped faults and the stratigraphic reflectors above the first water bottom multiple. Additionally, where primary reflections dip and the shallow multiple reflections are flat, stratigraphy can often be interpreted through the multiple reflections even in SCS data.

Faults in the Terror Rift were interpreted on all the seismic reflection data shown in Figure 2. These faults were correlated between reflection profiles and were digitally 3D viewed (Figure 5). Faults were drawn on fifteen depth-converted seismic reflection profiles (Figure S4). How the faults were correlated from one profile to the next is explained in the Supplemental text.

Velocity information for travel time to depth conversions were obtained by converting into interval velocities the stacking velocities of sub-horizontal reflections from processing of MCS data available on ANTOSTRAT (Brancolini et al., 1995a). Stacking velocities were converted into interval velocities using Dix's equation (Dix, 1995). Additional interval velocity information was obtained from sonobuoy refraction seismic data, retrieved from original publications and reports (Cochrane et al., 1992; F. J. Davey et al., 1982; Houtz & Davey, 1973; Sato et al., 1984) (for more information see supplemental data). We created 250 depth-time charts at sonobuoy locations and at selected stacking velocity points, which were located from just east of 180° longitude through the western shore of the Ross Sea (Figure 2). The depth-time charts were entered into the software IHS Kingdom Suite software. This software calculated

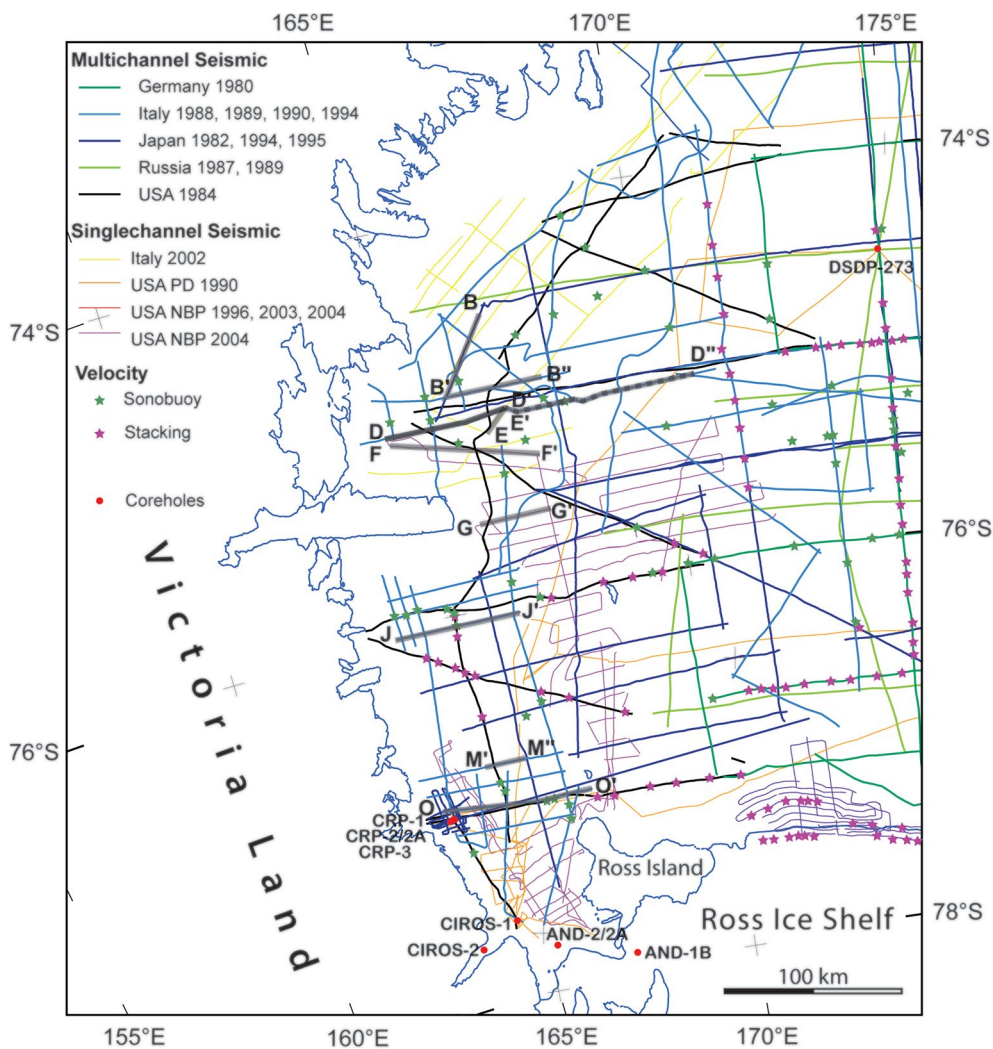


Figure 2. Location map of the seismic reflection tracklines, scientific drillholes, and depth-time charts derived from sonobuoys (green stars) or the interval velocities derived from stacking velocities (magenta stars). The seismic profiles shown in the following figures are denoted as B-B'-B'' through O-O'. The densely distributed depth-time velocity charts and thus the 3D velocity model and depth conversion cover this map and greater than 200 km to the east of this figure.

the average velocities for each unconformity grid at each depth-time chart. Gridding of the average velocities between control points produced average velocity grids from the sea surface to each digital unconformity grid. These were used to convert the travel time grids into depth. Time and depth grids were paired, including sea surface, sea floor, and subbottom grids, and a 3D velocity model was created in the IHS Markit Kingdom Suite. This 3D velocity model was applied to the seismic reflection profiles shown in Figures 6 and S4, and a depth version of each profile was created in the IHS Markit Kingdom Suite. The same velocity model was used to convert faults into depth. These depth faults were then displayed on the depth seismic profiles.

We analyzed how vertical motion was accommodated along 300 km of the Terror Rift. The components of the relative vertical relief between the western edge of our data and the deepest point of the basin, and between that basin and the highest part of the eastern rift shoulder, were measured on 15 depth-converted profiles, which are presented in the supplemental data (Figure S4). These measurements were summed for each flank of the rift, for each depth section, for both faulting and dip.

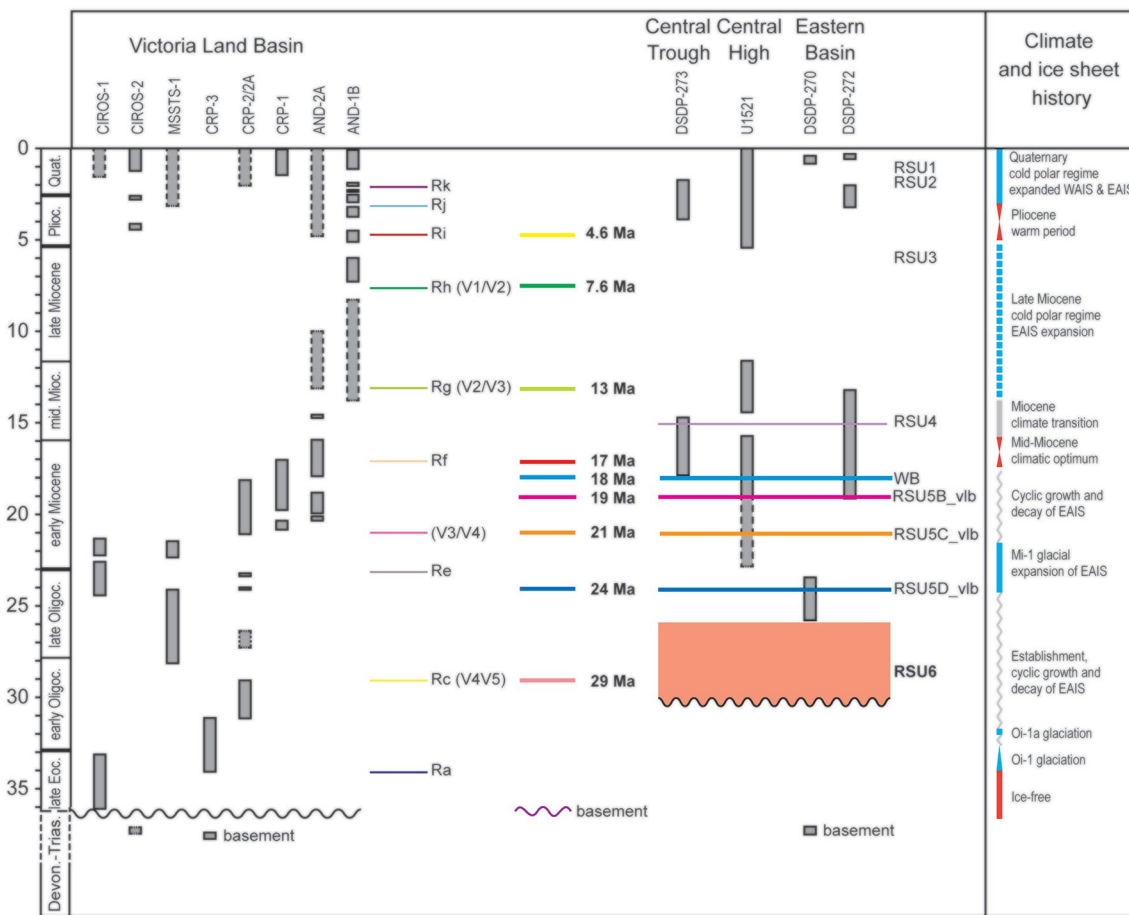


Figure 3. Time-distribution of the well stratigraphy and regional seismic reflectors/unconformities for the Ross Sea. Stratigraphy of the wells CIROS-1 (Barrett, 1986, 1989; Harwood, 1989; Sagnotti et al., 1998; G. S. Wilson et al., 1998) and CIROS-2 (Barrett and Scientific Staff, 1985; Winter & Harwood, 1997). CRP-1, CRP2/2A, and CRP-3 (Cape Roberts Science Team, 1998, 1999, 2000); AND-1B and AND2/2A (SMS Science Team, 2010); DSDP 270, 272, 273 (Hayes & Frakes, 1975; Savage & Ciesielsky, 1983) with updating of the DSDP 270 after Kulhanek et al. (2019). Seismic reflectors/unconformities interpreted in the Victoria Land Basin: Ra to Rk unconformities from Fielding et al. (2008); V1 to V5 from Cooper et al. (1987a); ANTOSTRAT Unconformities (RSU) RSU1 to RSU6 from Brancolini et al. (1995a, 1995b); Wb reflector at the bottom of DSDP 273 from Savage and Ciesielsky (1983), Sauli et al. (2014); RSU5B_vlb and RSU5C_vlb from this work and Brancolini et al. (1995a, 1995b); RSUD5_vlb from this work and C. Sorlien et al. (2019), Brazell, (2017); Reflectors 29, 21, and 17 Ma from Hamilton et al. (2001), R. C. Fielding (2018) (reflector 21 Ma also from Fielding and Thompson, 1999). Climate and ice sheet history from R. C. Fielding (2018). Time scale from the International Chronostratigraphic Chart 2019/05 (www.stratigraphy.org; Cohen et al., 2013). See Figures 1, 2 and 5 for drillhole locations.

3. Results

The Terror Rift trough formed within the older and broader Victoria Land Basin (Figures 4, 5, and 6) and trends N-S between $76^{\circ} 15'$ and $74^{\circ} 45'$ (Figure 5). The Terror Rift terminates to the north at $74^{\circ} 30'$ and bends to the SSE near $76^{\circ} 15'$ and continues with that trend, at least to Ross Island. The eastern rift border faults bend to the NW and the rift itself may die out or terminate at these NW-SE faults (Figures 5, 7, and 9). Figure 4 shows that the very deep and relatively narrow Terror Rift is much narrower than the other Ross Sea sedimentary basins, which are hundreds of kilometers wide.

The western margin of the Terror Rift partially coincides with the western margin of the Victoria Land Basin along the front of the Transantarctic Mountains (Figures 4 and 5). The eastern margin of the Terror Rift cuts the middle of the Victoria Land Basin such that there is a 60–100 km width of the Victoria Land Basin that was not significantly affected by post 30–26 Ma faulting (post-RSU6) and especially by post-24 Ma faulting (Figure 8).

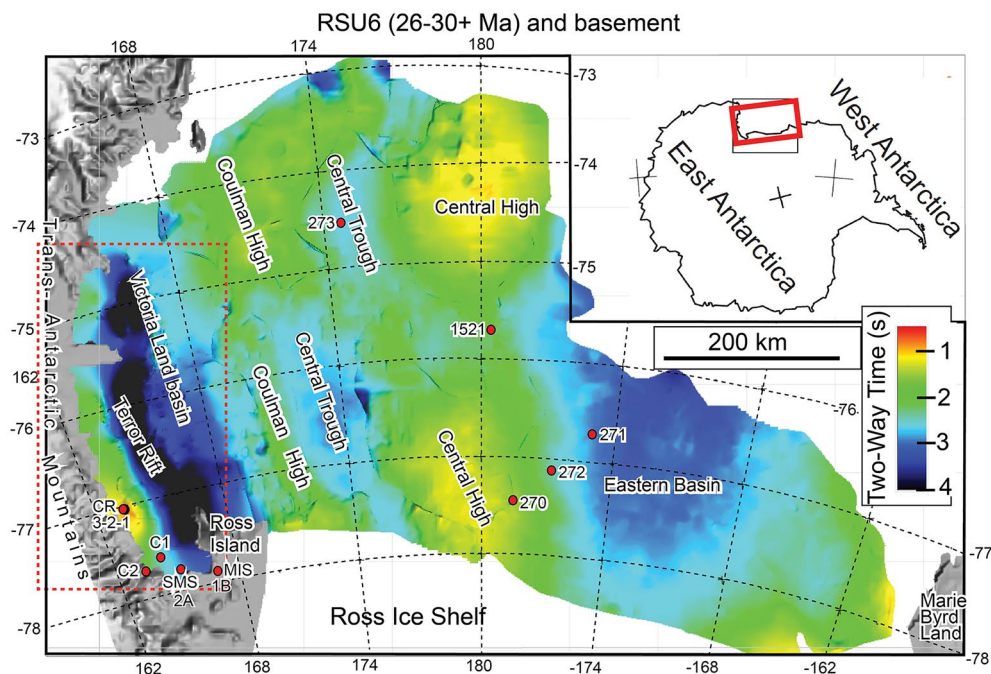


Figure 4. Ross Sea basins that are evident on the mid-Cenozoic RSU6 horizon. This horizon is deeper than 4 s two-way time in part of the Terror Rift. The scientific core holes are labeled with red dots: 270, 271, 272, and 273 are Deep Sea Drilling Project; CRP 3-2-1 are Cape Roberts Project; C1 and C2 are Ciros 1–2; MIS-1B and SMS-2A are Andrill and U1521 is IODP. The red dashed rectangle indicates the volume of Figure 5.

3.1. Stratigraphy

Our seismic stratigraphic correlations are part of a broader effort to interpret the Oligocene through middle Miocene reflectors by using all the available seismic reflection data from most of the Ross Sea (the area of Figure 4; C. C. Sorlien et al., 2016, 2019). This work continued and includes seismic stratigraphic correlations throughout the Victoria Land basin, which included the Terror Rift. The starting points were the ANTOSTRAT (Brancolini et al., 1995a, 1995b) interpretation at Deep Sea Drilling Program sites 270, 272, and 273. The ANTOSTRAT (Brancolini et al., 1995a, 1995b) stratigraphy contains eight seismic sequences that overlie the Mesozoic acoustic basement and are bounded by seven unconformities (e.g., RSU6 - RSU1) with ages ranging from Late Oligocene (RSU6) to Lower Pleistocene.

The C. Sorlien et al. (2019) RSU5 unconformity is 570 m below the bottom of DSDP site 273 in Central Trough, and at this location, it is nearly the same as the ANTOSTRAT (Brancolini et al., 1995a, 1995b) interpretation in two way time but is significantly deeper in depth. A revision of the depth and age of the RSU5 unconformity is ongoing after the recent IODP Expedition 374, which drilled site U1521; this site is located near the western edge of the Eastern Basin (Figures 1 and 4) and that reached sediments dated ca. 18 Ma near the bottom of the hole (McKay et al., 2019). Therefore, we used the names RSU5B_vlb (19 Ma) and RSU5C_vlb (21 Ma) labels in the Victoria Land Basin (extension “_vlb” stands for Victoria Land Basin). The ages of these reflectors are the same as the ages of the RSU4A and RSU5 unconformities from Brancolini et al. (1995a, 1995b).

In this paper we correlated different reflectors by using the published seismic stratigraphy nomenclature and ages assigned (Figure 3):

- The age of the unconformity RSU6 the age is > 26–30+ Ma on the basis of the sediments ages at DSDP 270 (Kulhanek et al., 2019) in the eastern Ross Sea, although this unconformity cannot be traced directly across the Ross Sea and its age may be diachronous from east to west. A potentially equivalent reflector labeled with age 29 Ma in the southern Terror Rift is correlated from the Cape Roberts core holes (Cape Roberts Science Team, 1998, 1999, 2000; F. J. Davey et al., 2000; R. C. Fielding 2018; Hamilton et al., 2001; Whittaker, 2005;)

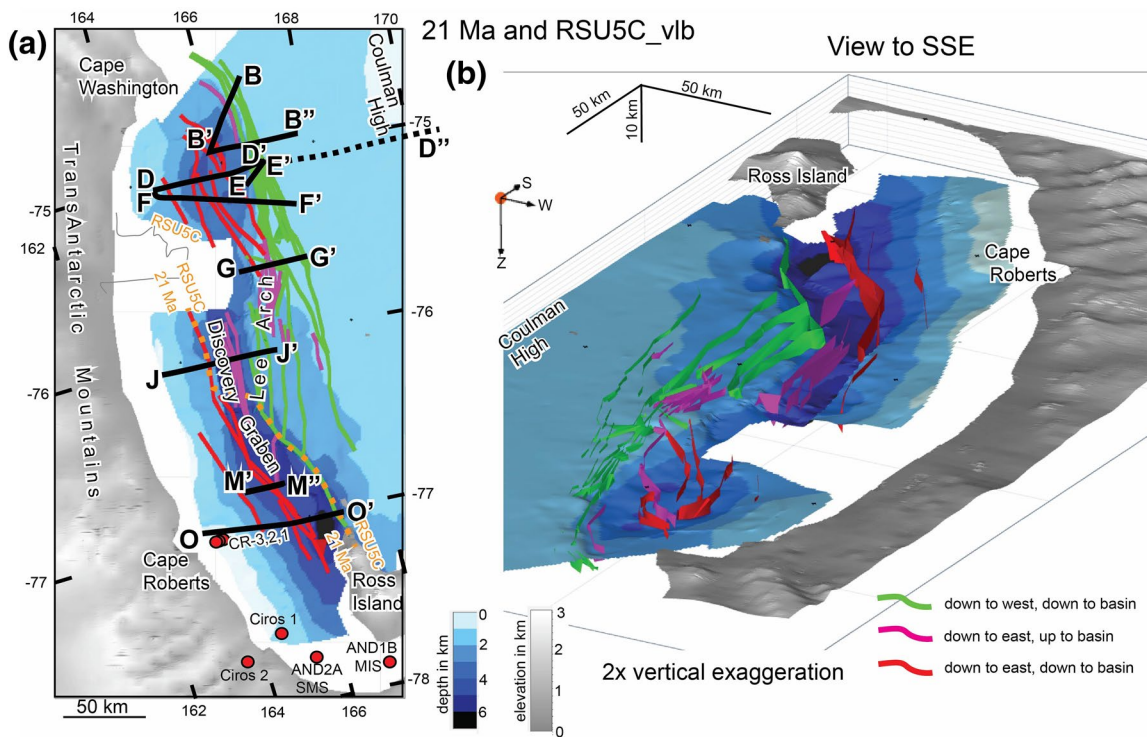
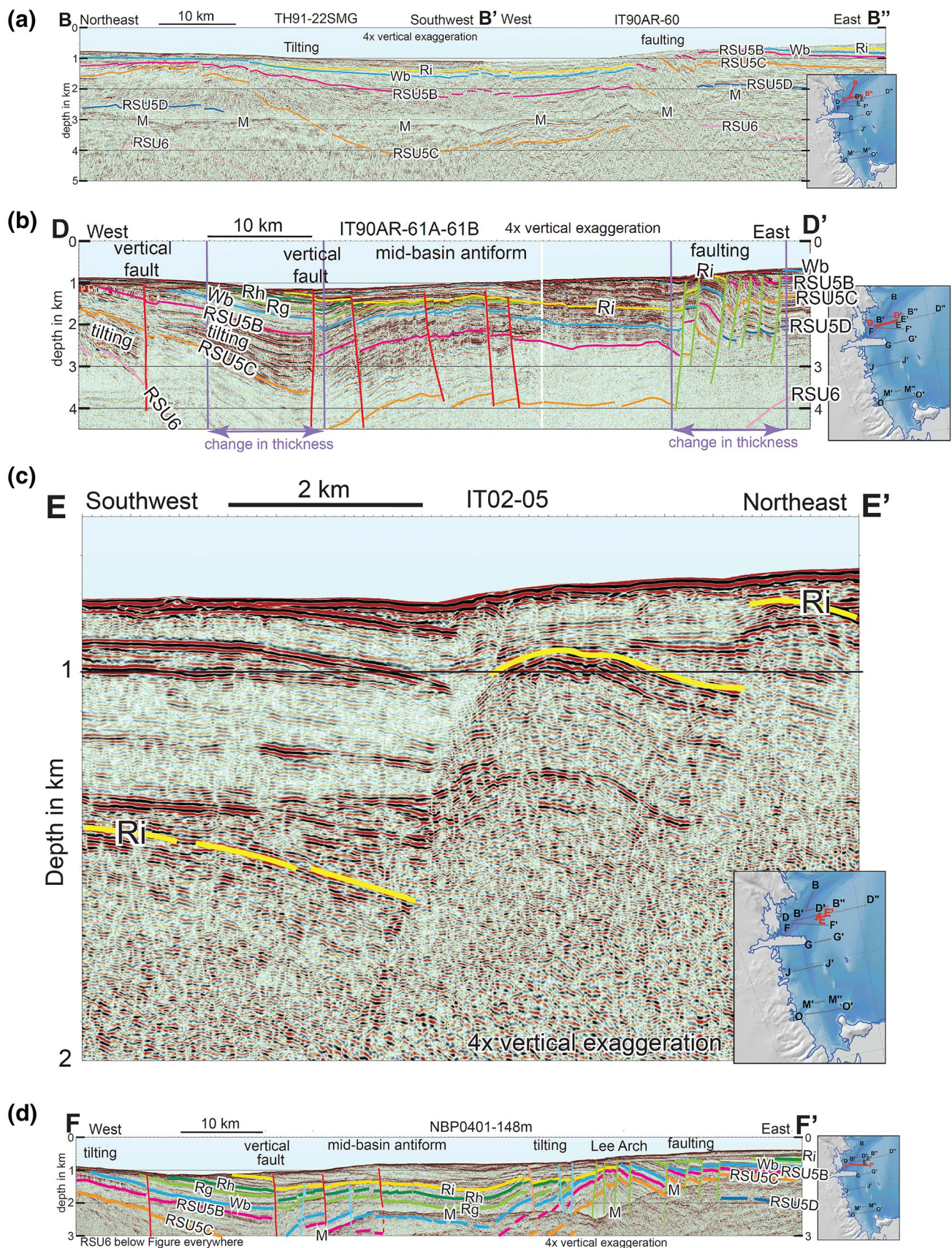


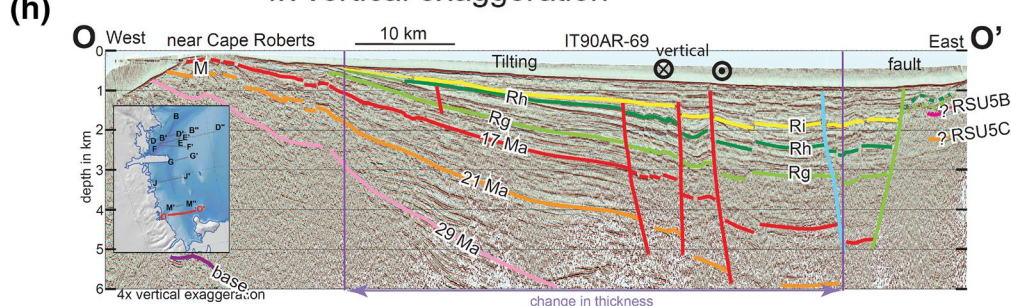
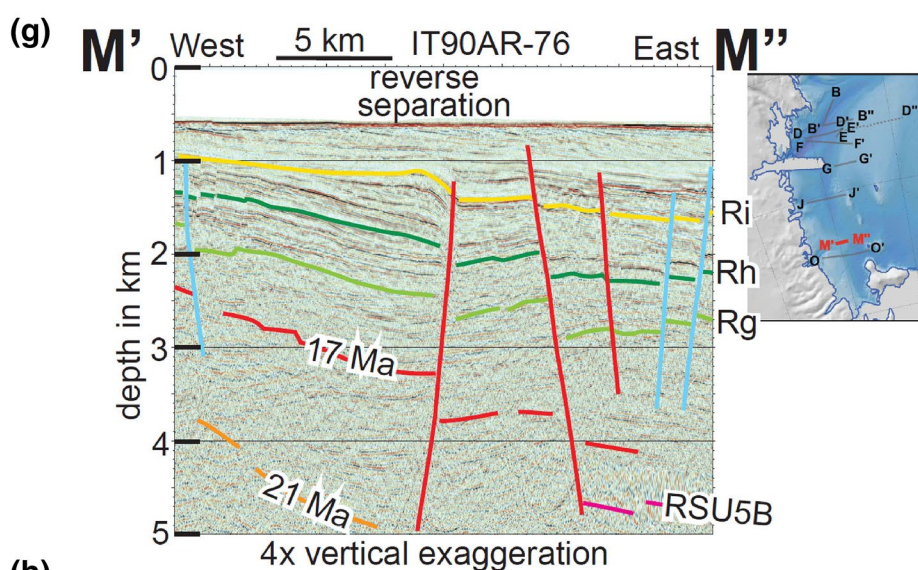
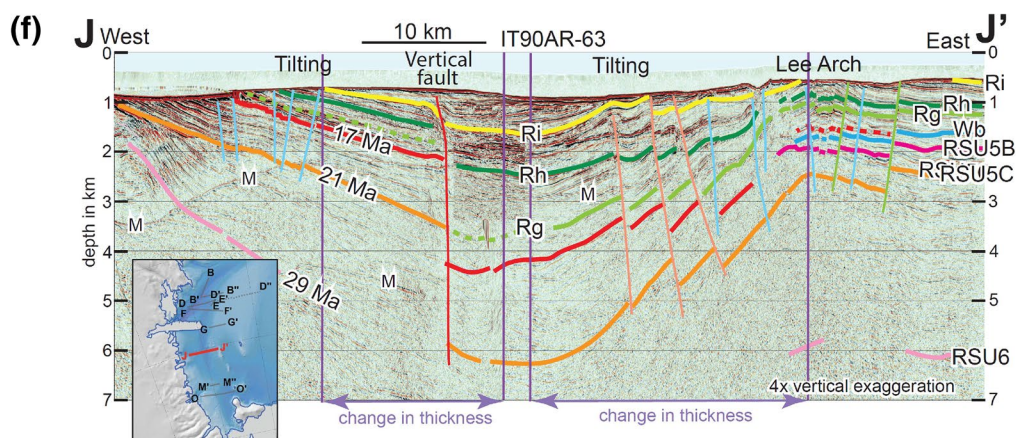
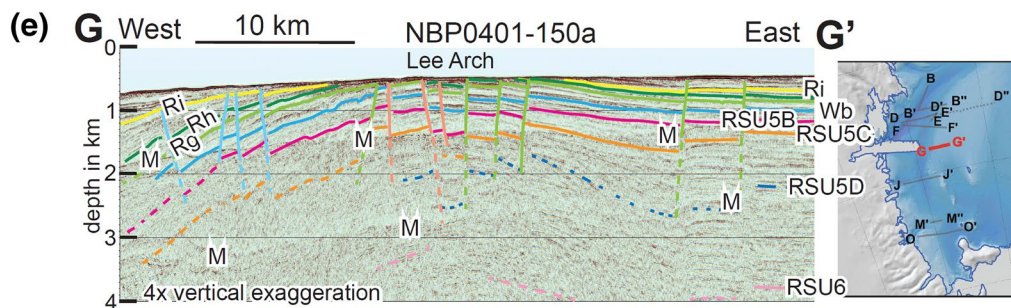
Figure 5. Plan (a) and oblique (b) views of the merged 21 Ma (west) and RSU5C_vlb (east) unconformities. The orange dashed line on the plan map (a), which mostly runs along two of the large faults, shows the limit of the merged unconformities. RSU5C_vlb and 21 Ma were correlated across the boundary as the same unconformity near the label "Graben." We acknowledge that this correlation has certain limitations, including interpretation of the vertical component across faults. These horizons and the faults are all displayed in depth with two times vertical exaggeration. The northern rift trends N-S, while the southern rift trends NNW-SSE. A large fault(s) may be present west of these grids along the front of the Transantarctic Mountains. The faults colors indicate the sense of vertical motion (red color =eastward and green color = westward).

- (b) Reflector RSU5D_vlb is tentatively correlated from the Eastern Basin into the northern Terror Rift and the eastern shoulder of the central and northern rift (Brazell, 2017; C. C. Sorlien et al., 2016). RSU5D_vlb is dated to ~24 Ma in DSDP-270 (Kulhanek et al., 2019)
- (c) We correlated from the Central Trough to the Victoria Land Basin reflectors RSU4A (19 Ma) and RSU5 (21 Ma) of Brancolini et al. (1995a, 1995b) and renamed them RSU5C_vlb and RSU5B_vlb respectively
- (d) Reflector Wb (well bottom of DSDP 273 of Sauli et al., 2014) is dated to ~18 Ma
- (e) In the southern Terror Rift the reflector at 29 Ma is from Hamilton et al. (2001) and R. C. Fielding (2018). The reflector dated to ~21 Ma is from Fielding and Thompson (1999), and Hamilton et al. (2001). The reflector dated to ~17 Ma is from Hamilton et al. (2001) and Fielding et al. (2018)
- (f) The reflectors labeled Rg with ages of ~13 Ma, Rh with an age of 7.6 Ma and Ri with an age of ~4.6 Ma are from correlations with the ANDRILL core holes (C. R. Fielding et al., 2006, 2008; R. C. Fielding, 2018; Horgan et al., 2005; Naish et al., 2007; Pekar et al., 2013). Wenman et al. (2020) used the age ranges of 10.8–13.6 Ma for reflector Rg, 7.3–7.8 Ma for reflector Rh and 4.0–4.6 Ma for reflector Ri based on work by G. Wilson et al. (2012) and Naish et al. (2007)

We have retained the different names and ages from core holes of these sets of stratigraphic nomenclatures in the text and in the figures. The RSU unconformities are correlated by using all the available data from the Eastern Basin across the Central High to the area of DSDP 273 in the Central Trough (Figure 4; Sorlien et al., 2016, 2019). They are all traced across the Coulman High and along the eastern shoulder of the Terror Rift, and into the northern part of the Terror Rift. RSU6 onlaps the acoustic basement on both sides of the Coulman High, and is correlated into the Victoria Land Basin via comparison of reflection patterns, with a similar interpretation to that of ANTOSTRAT (1995).

The unconformities labeled 29, 21, and 17 Ma are correlated from the Cape Roberts core holes into the deepest part of the Terror Rift, near the latitude of the core holes, and along the western flank of the southern





Terror Rift for 100 km northward. These unconformities were paired with the RSU unconformities from the eastern flank of the Terror Rift, based on their similar ages. The seismic stratigraphic correlation from the eastern rift shoulder into the deep basin was determined where the vertical component across faults was the least. The unconformities were correlated along profiles that were more parallel to the rift trend in the deep basin and on eastern rift shoulder. This loop-tying (supporting information and Figure S1) procedure allowed our stratigraphic interpretation across faults where the vertical components are greatest.

The Rg (~13 Ma) and Rh (7.6 Ma) unconformities were correlated from over-ice seismic reflection profiles in the McMurdo Sound area, as discussed in Pekar et al. (2013) and Wenman et al. (2020), northward within the basin, and to the eastern shoulder of the central and northern rift. The Ri unconformity (~4.6 Ma) could not be directly correlated north from the area near ANDRILL 2A, so we interpreted a regional unconformity farther north as Ri (Figure 3). This interpretation is the same as that of Fielding et al. (2008) for seismic line IT90-75.

The results of the scientific coring provided an age control for the reflectors that were correlated by use of seismic reflection data. In the following paragraphs the regional-scale deformations of the sedimentary rocks from differential subsidence, faulting, and folding are presented. The thicknesses of sedimentary rocks intervals are related to sediment availability and to the accommodation space produced by spatially variable subsidence. The thickness of the middle Miocene through lower Pliocene rocks is limited by the significant erosion on the rift shoulders as well as in the northern rift basin.

The upper Oligocene—lower Miocene section between RSU6 and RSU5C_vlb (29 Ma–21 Ma) is interpreted to be ~3 km thick in the center of the Terror Rift (extrapolated on profiles in Figures 5, 6b, 6f, and 6h). The late Oligocene and older strata thicken toward the Terror Rift from the Coulman High westward, and from the western shoulder eastward (Figures 6b, 6f, 6h, and 8). These strata clearly dip more steeply than the overlying Miocene sediments on the western rift flank. The reflectors diverge in a fan pattern from the western edge of our interpretations toward the basin center. This fan pattern is also observed between the eastern shoulder of the central rift and the basin, with reflectors diverging westward (Figures 6e and 6f). This pattern suggests a continuous subsidence across the Terror Rift, with the basin center subsiding most rapidly and with subsidence rates decreasing both east and west toward the rift shoulders. In addition to the E-W variation in sedimentary thickness, there is a N-S variation. The late Oligocene and younger section is thickest near Ross Island (Figure 5), thick in the central rift, and thinner in the northern Terror Rift (Figures 5, 6b, 6f, and 6h).

Figure 6. (a) Composite profile B-B'-B'', is displayed in depth and is shown in Figures 2 and 5. The profile crosses the same faults at two locations, which form the eastern shoulder of the northern Terror Rift. The subbottom vertical structural relief between B and B' is predominantly tilted, while 20 km to the south, the relief across the rift margin between B' and B'' is predominantly faulted. M is for multiples. (b) Profile D-D' is displayed in depth across the Terror Rift and is located in Figures 2 and 5. The subbottom structural relief of the western margin is predominantly tilted, with part of the relief formed by faulting. The relief of the eastern margin is fault dominated. The light and dark green Rg and Rh horizons are eroded away by Ri (~4.6 Ma) in part of the basin. Rg, Rh, and Ri are all eroded on both flanks of the rift by a post-Ri unconformity. Several million years of time is missing due to erosion of the Ri and post-Ri unconformities (also on B-B'-B'' in Figure 6a). The phrase “change in thickness” indicates where the measurements of thickness changes shown in the graph of Figure 11 were made. (c) Profile E-E' is the single channel seismic profile IT02-05, which is displayed in depth and is located in Figures 2 and 5. This profile crosses the northeastern margin of the Terror Rift and displays a 600 m vertical component of displacement of Ri across a single fault strand. Thus, there is Plio-Quaternary activity on these and other faults. Both imaged faults are associated with sea floor scarps or fault-line scarps. (d) Profile F-F' is displayed in depth and is located in Figures 2 and 5. The structural relief on both the east and the west are due to both tilting and faulting. As for D-D' profile, there is a broad gentle antiform in the middle of the rift basin. Large vertical components of offsets of Rh and Ri (~4.6 Ma) suggest Plio-Quaternary fault activity. This profile is displayed to 5 km depth in Figure S4e. M is for multiples. (e) Profile G-G' is displayed in depth and is located in Figures 2 and 5. Steep to subvertical faults with an inferred extensional slip component cut the broad rift shoulder anticline (Lee Arch). Most of the structural relief between the anticline and the deep basin to the west of the figure is tilted, while on most of the faults in the western 20 km of this figure, the vertical component is up-to-the-basin. (f) Profile J-J' is displayed in depth and is located in Figures 2 and 5. The subbottom structural relief of the western rift margin is formed half by tilting and half by faulting. The relief on the eastern flank is almost entirely tilted; indeed, most of the faults are upthrown toward the basin center. M is for multiples. The phrase “change in thickness” indicates where the measurements of thickness changes shown in the graph of Figure 11 were made. (g) Profile M-M', part of seismic profile IT90AR76 is displayed in depth and is located in Figures 2 and 5. This portion of a longer profile crosses the lower part of the western rift flank. The large western fault dips west and thus have reverse separation through the Miocene and younger sections. The next fault dips east and exhibits normal separation. Many minor faults deform the post-7.6 Ma sedimentary rocks. The full profile is presented in Figure S4l. (h) Profile O-O' is displayed in depth and is located in Figures 2 and 5. The ridge at the western end of the figure is near the Cape Roberts scientific core holes (Figures 1 and 2). The Terror Rift basin at this latitude is an asymmetric half-graben, and the structural relief is tilted in the west and is formed by a very large newly interpreted fault in the east. The 21 Ma horizon has a vertical separation of nearly 4 km across the eastern fault from the RSU5C_vlb horizon (21 Ma). Rh and Ri are also offset by the fault, which requires post-Miocene activity. The phrase “change in thickness” indicates where the measurements of thickness changes shown in the graph of Figure 11 were made.

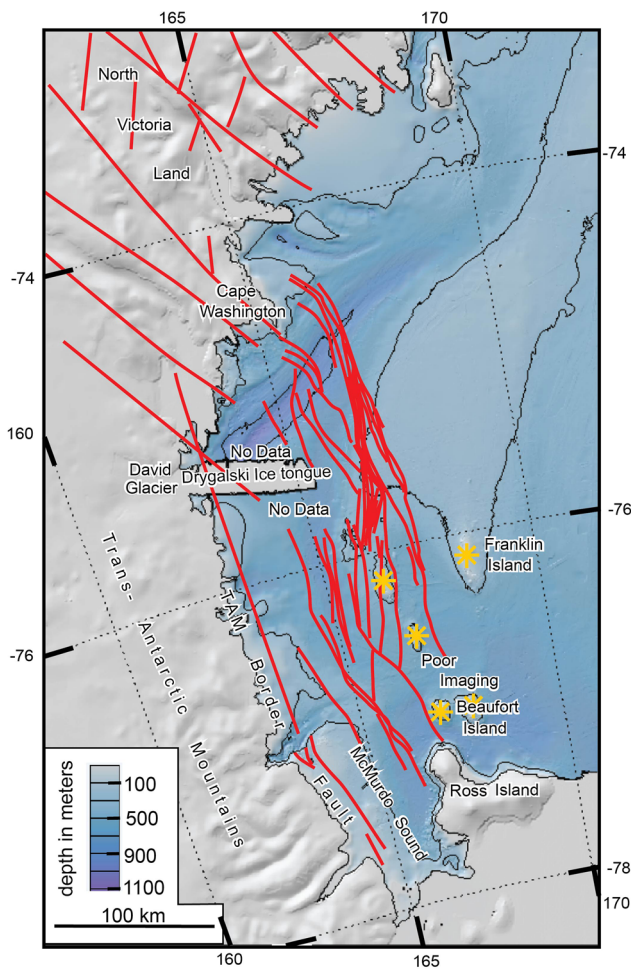


Figure 7. Map view of the interpreted faults. Faults are shown in red: onshore from Rosetti et al. 2006 and offshore from our mapping, except for the Transantarctic Mountains frontal fault system from Olivetti et al. (2018). The sea floor is displayed in shades of blue, and the main volcanic features are marked on the eastern Terror Rift flank with stars.

A part of the lower and middle Miocene section, namely, RSU5C_vlb–Rg (21 to ~13 Ma) dips more gently than the sedimentary section below within parts of the Terror Rift (Figures 6b, 6f, and 6h). This interval has a uniform thickness in the VLB east of the Terror Rift (Figure 8). The strata of this section are tilted and eroded on the western rift flank (Figures 6b, 6d, 6f, and 6h) and are tilted and significantly faulted on the eastern side, west of the Lee Arch (Figure 6f) and across the mid-basin antiform (Figures 6d and 6b).

The middle and upper Miocene sections, which are delimited by the regional unconformities Rg–Rh (~13–7.6 Ma), are significantly reduced in thickness in the northern depocenter with respect to the southern and central depocenter (Figures 6a, 6b, 6d, and 6h). This interval is thin or completely eroded away at or immediately below the sea floor along the eastern rift shoulder, including at the crest of Lee Arch (Figures 6b, 6d–6f, and 6h). This interval is also mostly or completely eroded away within the northern deep basin, especially on the Mid-Basin antiform (Figures 6a and 6b). The erosion of the Miocene to Early Pliocene sedimentary section at the northern edge of the Terror Rift, might have been caused by repeated ice-sheet oscillations over the past 13 Ma that were reported at the AND-2A (McKay et al., 2009; Naish et al., 2009).

In the northern Terror Rift the inferred Ri unconformity (~4.6 Ma) is interpreted as a subhorizontal erosional unconformity within the basin and on the eastern rift shoulder where it is not eroded away. The vertical component of the offset of Ri by faults is between 500 m and 1 km (Figures 6a–6c). Many faults offset Ri throughout the Terror Rift (Figure 6), and it is also involved in tilting (Figures 6e and 6h).

3.2. Faulting

On the eastern flank of the Terror Rift we interpreted different sets of faults with NNW-SSE and N-S striking directions. The NNW-SSE striking faults (i.e., the green fault set at the northern and southern rift ends in Figure 5 and segments 1, 3, and 4 in Figure 9) consists of down-to-basin normal-separation faults. The N-S striking faults (green and pink fault sets in Figure 5, segment 2 in Figure 9) are normally separated with both down-to-basin and up-to-basin stratigraphic separation, dissect the

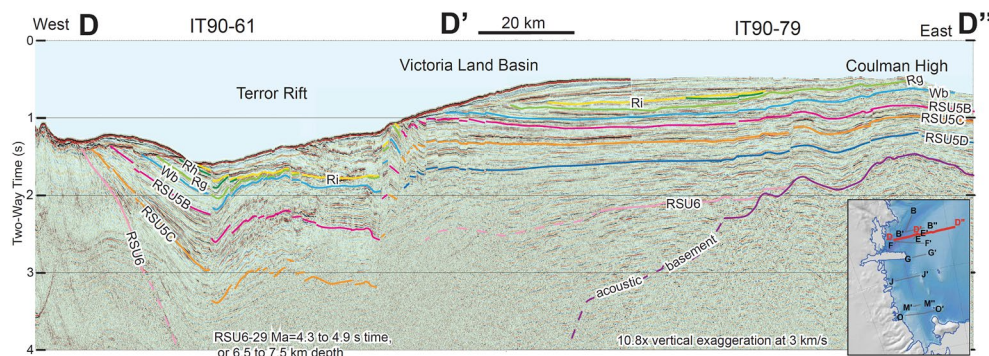


Figure 8. Composite multichannel seismic reflection profile across Terror Rift, Victoria Land Basin and Coulman High, displayed in two-way time and located in Figures 2 and 5. The part of this profile between D and D' is displayed in depth with less vertical exaggeration in Figure 6b. The entire profile images the Terror Rift (TR) within the older Victoria Land basin (VLB). There has been little deformation east of the Terror Rift since RSU6 (26–30+ Ma), and even less after RSU5D_vlb (24 Ma), even while the Terror Rift experienced two to 3 km of relative vertical motion here.

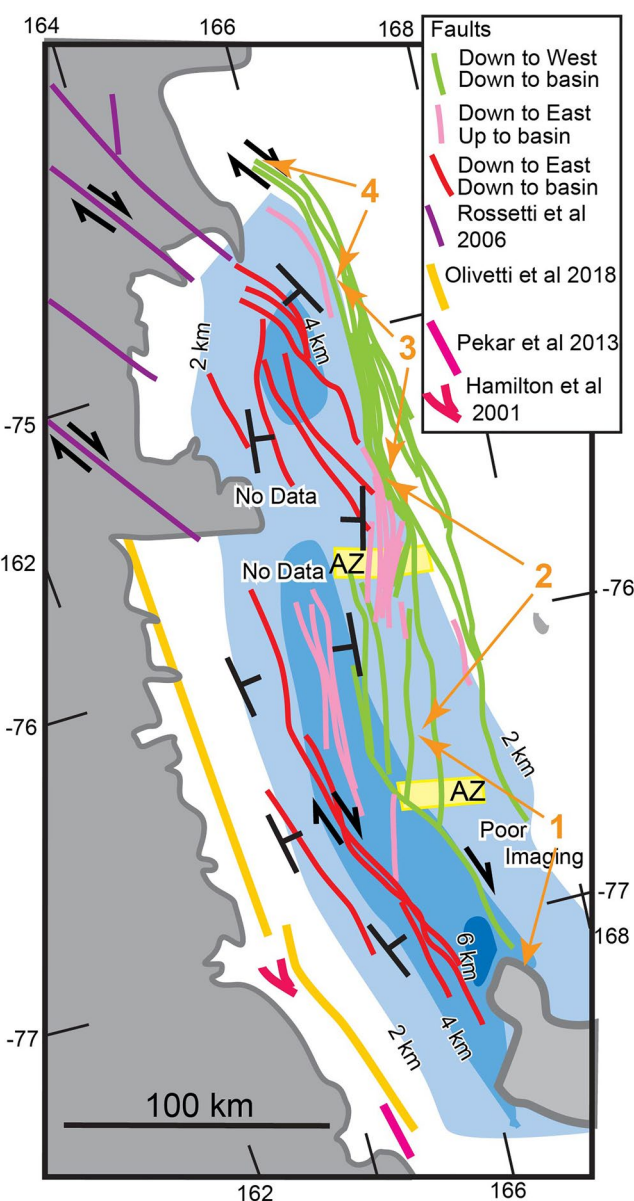


Figure 9. Oblique rift model for the Terror Rift. The black dip symbols indicate rift margins that tilt progressively down-to-the-basin. Darker blue and light blue colors represent deep and deeper rift basin sectors, respectively. The rift trends N-S for most of its length but trends NNW-SSE in the south and dies out on the north near the NW-SE faults, which were interpreted as right-lateral by Rossetti et al. (2006). The “AZ” symbols indicate the eastern parts of the accommodation zones of. The orange 1, 2, 3, and 4 numbers refer to the segmentation of the eastern rift boundary (see the text for more explanation). The yellow fault is the Transantarctic Mountains (TAM) Border Fault modified from Olivetti et al. (2018). It is only inferred along most of its length, but is imaged in small areas on the south of the figure.

4. Discussion

In the following paragraphs we discuss the results of our comprehensive interpretation with their geological implications and in light of previous published models. This discussion includes geometry, stratigraphic architecture, and kinematics over time for all the 350 km of the portion of the Terror Rift north of the Ross Ice

eastern Terror Rift margin and connect the NNW-SSE faulted margins to the south and north through a broad anticline (Lee Arch of Cooper et al., 1987a).

On the western flank of the Terror Rift, there is an NNW-SSE striking set (i.e., the red fault set in Figures 5 and 9) of steep to sub vertical faults, which locally exhibit reverse separation (Figure 6g). The largest of these down-to-basin faults delimits the deep rift basin center and dissect the mid-basin antiform in the north (Figures 6b and 6d). Our work does not include the Transantarctic Mountains (TAM) Border Fault (Pekar et al., 2013), along the western uplifted Ross Sea rift flank (McMurdo Sound Fault Zone of Hamilton et al., 2001; Figures 7 and 9).

The overall geometry of the Terror Rift graben varies spatially from south to north. The rift displays a half graben structure in the south with the main bounding fault located on the east side (Figure 6h). Part of the central rift includes a half graben with the main bounding fault located on the west side (Figure 6f). Northward the graben becomes symmetric with a broad flatter basin center (segments 3 and 4 in Figures 6b, 6d and 9).

Some faults exhibit reverse separation of strata, while others are subvertical (Figures 6b, 6d–6h). Most nonvertical faults exhibit normal separation for all pre-Pliocene stratigraphic horizons, with larger separations for older horizons than for younger horizons. There are local fault strands with reverse separation that strike parallel to those with normal separation (Figure 6g).

The depth-converted MCS profiles that cross the Terror Rift are presented from north to south (Figures 6a–6h). These profiles show how the vertical relief was accommodated on the rift flanks. On the northeastern border, a change in vertical relief accommodation from tilting to faulting occurs within a 30 km distance (Figure 6a). Farther south, along the eastern rift flank, the accommodation is dominated by a series of seven faults (Figure 6b) and changes southward, where it is almost entirely dominated by tilting, with most of the faults being up-to-basin (Figures 6e and 6f). On the southeastern border, nearly all of the relief occurs across one narrow fault zone that delimits a half graben (Figure 6h).

The vertical relief between the Terror Rift margin and its axial basin is taken up by a combination of tilting and faulting along its western flank and by a spatial alternation between faulting and tilting along strike on its eastern flank, which forms discrete segments (Figure 9). Where the vertical relief between the rift shoulder and basin is mainly due to faulting, the stratigraphic separation, as expected, is down-to-basin (profile D-D', Figure 6b). However, on those segments where the down-to-basin relief is due to tilting, there are zones of up-to-basin faults that dip away from the middle of the basin and toward the rift shoulder (profiles F-F', G-G', J-J', Figures 6d–6f). These faults mostly strike north and link the northern and southern eastern rift border faults (Figures 5, 7, and 9). Unconformities can be correlated in the seismic reflection data across the tilted boundaries and then correlated on both sides of the faults to demonstrate the vertical separation across the fault boundaries.

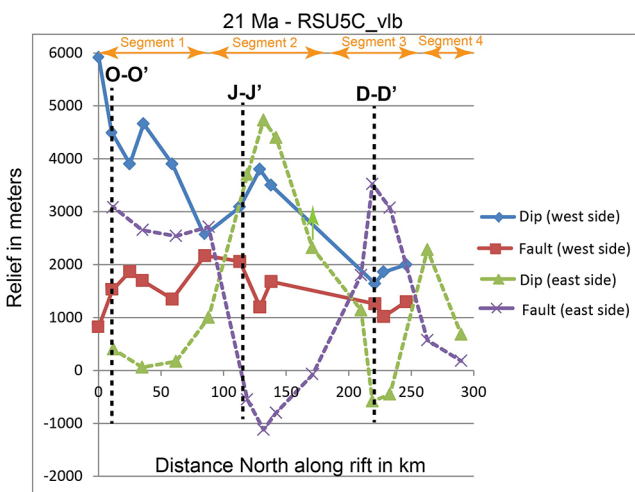


Figure 10. Components of Terror Rift relief due to faulting and due to dip for the eastern margin (dashed) and western margin (solid). The positive dip on the eastern side is to the west, while the positive dip on the western side is to the east. The eastern margin has four segments, where the relief alternates between faulting and dip. The western margin relief is due to both faulting and to dip, except in the south, where it is mostly due to dip. Relief on the western margin does not include any proposed fault system between the Transantarctic Mountains and the Ross Sea.

where the vertical relief is due to dip (Figures 5, 9, and 10). This dip segment (numbered 2 in Figure 9) is cut by N-striking faults with a vertical relief up-to-basin. This segment also includes southward diverging down-to-basin faults east of the crest of the Lee Arch (Figures 6d–6f). The segment is separated from the northern fault segment (numbered 3) by a discontinuity interpreted as a WNW-striking accommodation zone by Hall et al. (2007) (Figure 9). In their interpretation of the northern accommodation zone, which coincides with ours, Hall et al. (2007) included an ~23 km right step or offset of fault zones, anticline axes, and the deep basin center across this zone. Instead of interpreting this lateral offset across the accommodation zone, we map a double right bend of ~7 km (Figures 5 and 9). This broad double bend is dominated by down-to-the east faults that we map as continuous across the Hall et al., (2007) accommodation zone. There are no data to constrain the deep basin at the accommodation zone. Simply gridding the interpreted 21 Ma horizon produces no offset of the deepest basin there (Figures 5 and 9).

The anticline zone (Lee Arch), on the eastern border of the Terror Rift, is dissected by N-S-striking up-to-basin and down-to-basin steep to subvertical faults (Figures 6d–6f). This kind of geometry can form during an orthogonal extension, such as a rollover fold in an extensional basin (Withjack et al., 1995; Xiao & Suppe, 1992). Nevertheless this geometry is also similar to a negative flower structure, where faults with opposite dips converge downward (e.g., Sylvester, 1988), and are often interpreted to be diagnostic of strike-slip motion (Lowell, 1972; Ramsay & Huber, 1987; Sylvester 1988). The relation of faulting to the northern part of Lee Arch anticline is seen on F-F' profile (Figure 6d). The western limb of the anticline can be explained as due to the more rapid subsidence of the deepest part of the Terror Rift that resulted from crustal thinning, thermal contraction, and sediment loading. The eastern limb exhibits back tilting into the imaged normal-separation faults. These faults may or may not be bookshelf faults, rotating about a horizontal axis, above an inferred gently-dipping detachment below (Mukherjee & Khonsari, 2018). Such a detachment is not imaged, but gently-dipping faults are expected in a location that extended for 100 km (Fossen et al., 2000). The same mechanism could explain the similar anticline as imaged on G-G' (Figure 6e), where the back-tilting into west dipping faults is less obvious.

The west dipping fault on the southernmost O-O' profile shows nearly 4 km of normal vertical separation of the ~21 Ma unconformity in the half-graben basin, to the RSU5C_vlb reflector (21 Ma) on the east footwall of that fault (Figure 6h). We advocate that the down-to-east tilting could partly be back tilting into this

Shelf edge. We briefly consider the evidence for Plio-Quaternary tectonic activity in the study area and present our results for measured post-21 Ma and post-13 Ma crustal extension in the Terror Rift.

4.1. Geometry of the Terror Rift

How the vertical relief of reflectors is accommodated is different in the west versus the east, and it varies in four segments along the eastern flank. The vertical relief across the western flank of the Terror rift is due to both a stratal dip and faulting, without distinct segmentation along the trend (Figures 9 and 10). The vertical relief due to faulting ranges between 1 and 2 km, as measured for the 21 Ma horizon (Figure 10, solid red line), while the vertical relief due to dip increases from near 2 km in the north to 6 km in the south (Figure 10, solid blue line). This does not include any possible additional relief that is present west of the available offshore seismic reflection data along the front between the Transantarctic Mountains and offshore basin (Figures 7 and 9). It can be hypothesized that the Victoria Land Basin and the deeper inner Terror Rift share their western rift boundary near the current coastline along both interpreted and inferred faults (Ferraccioli et al., 2009; Hamilton et al., 2001; Pekar et al., 2013).

The eastern flank of the Terror Rift is partitioned into four structural domains, which alternate between accommodating the vertical relief into the basin by either tilting or faulting (Figures 9 and 10). The fault-controlled segments (numbered 1 and 3 in Figure 9) are linked by a segment

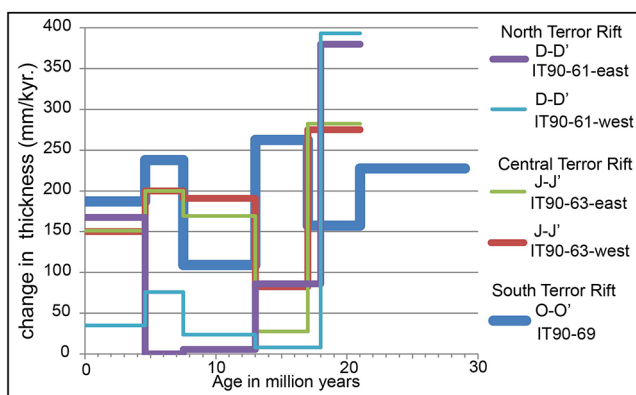


Figure 11. Measurements of sediment thickness changes over time in the Terror Rift. These measurements were made along the O-O' profile in the southern Terror Rift and are related to the western flank, along profile J-J' in the central Terror Rift, and along profile D-D', in the northern Terror Rift, which are both related to the eastern and western rift flanks (see Figures 6b–6h for measurement location). The sediment thickness changes are high between 29 and 13 Ma in the south and are smaller between 17 and 13 Ma in the central Terror Rift and after 18 Ma in the north.

tween 26 and 11 Ma across the Victoria Land Basin (Granot & Dymant, 2018). We have not interpreted significant Miocene activity or tilting across the eastern Victoria Land Basin (Figure 8), so the displacement was probably accommodated within the Terror Rift.

Some global strike-slip fault zones have vertical components that do not increase consistently downwards into older sedimentary rocks. These strike-slip faults can even vary within a short distance from normal to reverse separation with switching of the side that is downthrown, such as for the Palos Verdes fault near Los Angeles (Brankman & Shaw, 2009; C. C. Sorlien et al., 2013), and the Newport-Inglewood fault also near Los Angeles (C. C. Sorlien et al., 2015). In contrast, we interpret that even the subvertical fault strands have the same sense of vertical stratigraphic separation along their full lengths, and this vertical separation increases with depth and thus ages at any one location on a fault strand. While these observations do not support strike-slip motion, they also do not rule it out.

4.2. Stratigraphic Architecture and Passive 23–13 Ma Thermal Subsidence versus Ongoing Faulting and Tectonic Subsidence

Several publications have proposed that in the southern Victoria Land Basin, the sedimentary fill recorded passive thermal subsidence between 23 and 13 Ma, followed by renewed rifting activity after 13 Ma (R. C. Fielding 2018; Fielding et al., 2008; Henrys et al., 2007). Our results do not support the concept of an early Miocene interval of rift inactivity. We infer a continuous tilting over time between ~29 Ma and present in the southern Terror Rift and between 21 and 17 Ma in the central Terror Rift (Figure 11). This continuous tilting activity exhibits a segmented distribution on the eastern rift flank, and a spatial variation when moving northward on the west rift flank (Figures 9 and 10).

We cannot be confident of the possible differential vertical motion between 29 and 21 Ma across the central and northern Terror Rift because RSU6 (29 Ma) is poorly imaged to nonimaged in the deep basin and is mostly extrapolated below the younger horizons. However, the tilting between RSU6 (29 Ma) and RSU5C_vlb (21 Ma) or the 21 Ma horizons on the western part of the D-D' and J-J' profiles (Figures 6b and 6f) implies that differential vertical motion by tilting and probably by faulting also occurred on this flank of the central and northern Terror Rift. The thickness between RSU5C_vlb (21 Ma) and Wb (18 Ma) is much greater in the basin than on the rift shoulders on both the eastern and western margins, as displayed in the B-B' and D-D' profiles (Figures 6a and 6b). This dramatic decrease in thickness across the eastern rift

major fault (Figure 12). Normal slip on a fault interpreted as listric by R. C. Fielding (2018) is expected to produce such back tilts. In the southern Terror Rift, many profiles, such as O-O', end near this fault, and our interpretation of the stratigraphy across the fault is limited. Thus, we do not directly know the timing of the middle Miocene and younger activity across this fault or of the pre-21 Ma activity across it. However, the continuous back tilting started before RSU6 (29 Ma) and continued after Rh (7.6 Ma), which suggests continuous activity on the fault. We tentatively interpret ~1 km of vertical separation for Rh (7.6 Ma) across this fault. Similarly, Ri is truncated by this fault, and there is a minimum of a half kilometer of vertical separation across it. The fault reaches close to the sea floor and may have even been active during the Quaternary. The large vertical component of offset component and its association with the tilting of the half-graben does not preclude a similar or larger right-lateral component of motion across this fault.

Vertical faults, and steep faults with reverse separation are imaged in the northern and southern parts of the Terror Rift (west side of Figures 6b–6d, 6f, and 6g). Such a geometry suggests that they are strike-slip faults. The most conclusive evidence that supports the strike-slip motion comes from the quantitative analysis of marine magnetic anomalies by Granot and Dymant (2018), which results in an estimate of 30 km of transtensional right-lateral motion, and between 0 and 20 km of extension be-

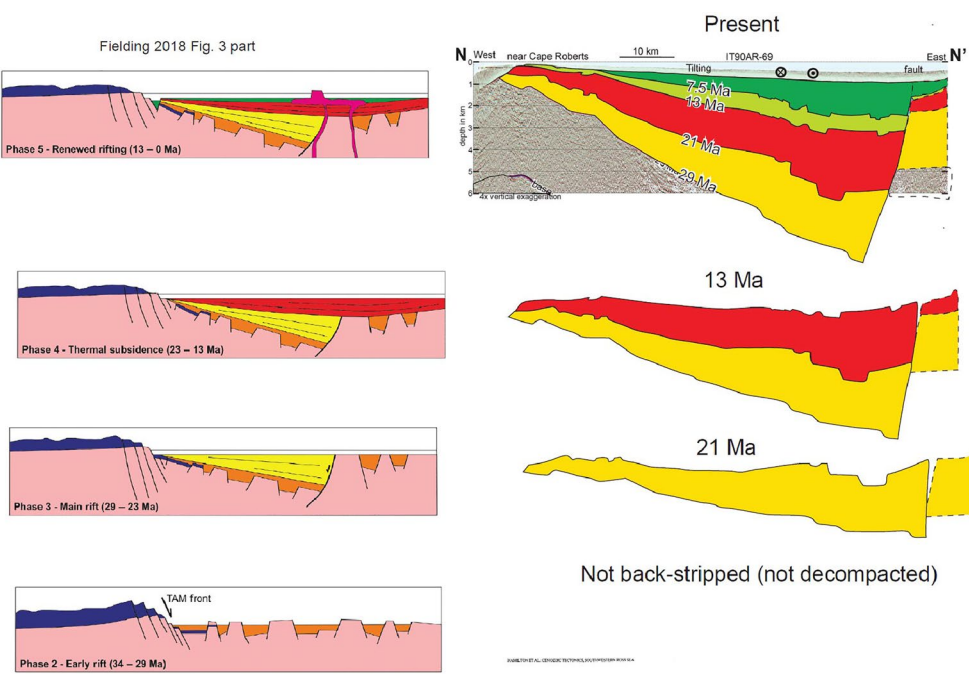


Figure 12. Comparison between the R. C. Fielding (2018) diagram on the left and our depth section, as observed in Figure 6h, on the right. The changes in sediment thickness across the fault show that there was growth on the fault and a faster vertical relief from 29 to 13 Ma than from 13 to 0 Ma (see also Figure 11).

border faults between 21 Ma and 18 Ma implies fault activity during this time interval (Figures 6a and 6b). Similarly, the changes in thickness due to tilting for this same age interval are evident in the F-F', G-G', and J-J' profiles (Figures 6d–6f) in the northern and central Terror Rift. Additionally, the thickness between ~18 Ma or ~17 Ma and Rg (13 Ma) is greater in the basin than on both rift shoulders in the northern and southern regions, as observed in the F-F' and O-O' profiles (Figures 6d and 6h). This thickness increase is much less dramatic than the thickness change for the interval below, in part because of the removal of part of this interval by later erosion (Profiles B-B', D-D' in Figures 6a and 6b).

In conclusion, due to the evidence of tilting and fault activity in the southern Terror Rift between 29 and 21 Ma, in the northern Terror Rift between 21 Ma and 18 Ma, and in southwestern and central Terror Rift continuously since 29 Ma, it seems likely that the entire rift was active during these time intervals.

The graph in Figure 11 shows the differences in the current compacted sedimentary rock thicknesses between locations on the rift shoulder and in the deepest part of the sedimentary basin over time. The measurements at the eastern and western boundaries of the central and northern rift were made on profiles J-J' and D-D' (Figures 6f and 6b), where the location of the measurements are indicated. The thickness changes of sedimentary rocks in the southern rift were measured only on the western flank of the profile O-O' (Figure 6h) with the reported location of the measurements. Sedimentary rocks for a given age interval were compacted more by deeper burial in the deepest basin than on the flanks of the rift. Therefore, our measures of the thickness changes of these sedimentary rocks underestimate the differences in the rates of sediment accumulation between the deep basin and the rift flanks. These thickness changes across faults provide information on the rate of the vertical slip components throughout the analyzed time intervals and can be considered in light of the interplay between slip rates, the regional subsidence and the sedimentation rate (Doglioni et al., 1997).

The resulting graph shows a high rock thickness change rate in the southern Terror Rift between 29 and 13 Ma, with the slowest rate being between 13 and 7.5 Ma. The central rift has a large change in rock thickness between 21 and 17 Ma, a low rate between 17 and 13 Ma, and a higher rate between 13 Ma and the present. This is true for both the eastern flank and part of the western flank and include a large fault. Thickness changes in the northern rift are high between 21 and 18 Ma and then are very small until 4.6 Ma. The rate

increases after 4.6 Ma on the eastern flank. In summary, thickness changes decrease after 17 or 18 Ma in the central and northern rift, while thickness changes decrease between 13 and 7.5 Ma in the southern rift.

These thickness changes are related to both the vertical motions of faults and to tilting and hence to the tectonic activity that affected the Terror Rift mostly between 29 and 13 Ma or between 21 and 18 Ma in the southern and northern sectors. Decreased tectonic activity appeared to occur, at least for the southern Terror Rift, when the renewed Terror rifting phase had been proposed by many authors (e.g., Fielding et al., 2008). The two hiatuses in thickness change for the periods of 18–4.6 Ma and 17–13 Ma and, in particular, the hiatus in the northern Terror Rift may have resulted from the influence on sedimentation of glacial discharge/erosion during the periodic Miocene oscillations of the David Glacier, which streamed preferentially within the northern part of the Terror Rift. Moreover, the greater thickness change rate after 4.6 Ma may in part be related to postglacial isostatic rebound at the rift flanks.

The depositional history of the southern Terror Rift after 29 Ma to the present is reconstructed during continuous rifting along the depth profile O-O' (Figure 6h), which is comparable, for the location, to the R. C. Fielding (2018) diagram (Figure 12). His reconstruction was simplified, and no decompression of the sediments was considered. In our depth profile, the tilt rate is constant, with no major changes after 29 Ma. The figure clearly displays the continuity of subsidence and faulting, which implies continuous synsedimentary deposition, with sediment strata that thicken basinward and with no significant major changes in the geometry of the basin infill over time.

Some portions of the subsidence that are associated with tilting result from differential thermal subsidence and sediment loading. However, without full basin modeling, it is not possible to guess the percentage of tilting due to this process versus that due to active extension. Such modeling would include the removal of both the sedimentary and water loads (backstripping), thermal subsidence related to the cessation of the rapid 43–26 Ma extension, and isostatic correction using a realistic elastic thickness of the Terror Rift crust if flexure is corrected for (Allen & Allen, 1990; Steckler & Watts, 1978; Watts & Ryan, 1976). Alternatively, Airy (local) isostatic correction would be performed. If the subsidence between, for example, 23 and 13 Ma can be fully explained by such modeling, then extension and crustal thinning are not required.

4.3. Evidence for 11 Ma to Present Tectonic Activity

Fault and tilt activity continued after 11 Ma, which is the age that Granot and Dyment (2018) proposed that East and West Antarctica became one plate. Published seismic reflection data have imaged late Miocene and younger sedimentary rocks being offset and deformed by faults that possibly reach the seafloor (Fielding et al., 2008; Hall et al., 2007; Hamilton et al., 2001; Henrys et al., 2007).

We present profiles E-E' and D-D' (Figures 6c and 6b, respectively), which show 800 m of vertical separation for unconformity Ri (~4.6 Ma) across two faults that have sea floor scarps or fault-line scarps. There are several hundred meters of additional vertical separation across the adjacent four large faults of Ri (Figure 6b). These profiles are located in the northern Terror Rift and we acknowledge that some of the fault movement may be related to glacial isostatic adjustment after late Pleistocene deglaciation (Hampel et al., 2010). The grounded David Glacier extended in the northeastern Terror Rift, and the stresses released since the Last Glacial Maximum during the postglacial unloading and rebound processes may be responsible for some of the fault movement. However, there have been numerous advances and retreats of this glacier and of the ice sheet during and after Middle Miocene time. These faults exhibit an increasing vertical offset component of the older rocks, which cannot be easily explained by glacial isostatic adjustment.

Our overall interpretation suggests the presence of Plio-Quaternary and possibly Holocene fault activity and is consistent with other geological evidence, such as volcanism within the Terror Rift and on its flanks (Giggenbach et al., 1973; P. R. Kyle 1990; P. R. Kyle et al., 1992; LeMasurier, 1990; Rilling et al., 2007; Rowe et al., 2000), and the high heat flow measurements (Blackman et al., 1987; Della Vedova et al., 1992, 1994).

4.4. Extension Across Terror Rift Since 21 Ma

To evaluate the crustal extension across the northern and southern Terror Rift since 21 Ma, the horizontal offset components of the faulted 21 Ma horizon were measured along the seismic depth profiles across the

rift. These measurements were carried out by summing the heaves across the faults along the profiles. The profiles are close to being perpendicular to the strikes of most of the faults, so the apparent extension due to faulting is sufficiently close to the true extension.

The measured extension of the RSU5C_vlb (21 Ma) horizon across the D-D' profile in the northern Terror Rift (Figures 6b and S5b) indicates 2.0 km of extension, while the post-21 Ma extension across L-L' in the southern Terror Rift (Figure S5a) is 3.6 km; additionally, an unknown amount of extension was accommodated by diking beneath a volcanic feature located east of L-L' and by an unknown amount of extension across the TAM Border fault(s).

Our interpretation indicates only a few km of post-21 Ma extension and indicates a significant change in the Terror Rift dynamics from the earlier nearly orthogonal extension to an oblique extension or transtensional motion (Granot & Dyment, 2018; Granot et al., 2013).

5. Summary and Conclusions

We present the geometry of the entire 400 km length of the Terror Rift, which is located north of the ice shelf edge. The stratigraphy dated at core holes, which was correlated through grids of seismic reflection profiles, allowed the sedimentation and relative vertical motion over the last 29 million years to be studied. Published plate tectonic studies combined with our interpretation of subvertical faults suggest that the Terror Rift was spatially focused within an older broader basin at ~26 Ma, as oblique rifting and transtensional strike-slip faulting replaced earlier nearly orthogonal rifting. The vertical relief was accommodated differently on the two opposite rift flanks and was spatially different among the four segments along the eastern flank. The entire western side of the Terror Rift, which is along the Transantarctic Mountain front, was formed by a combination of both faulting and tilting, with tilting forming most of the vertical relief in the south. The eastern side is segmented into four segments that exhibit alternate faulting and tilting. A broad anticline in the southern tilting segment is dissected by steep to subvertical faults that converge downward and form a strike-slip flower structure geometry. The geometry of the Terror Rift varies spatially from a southern and central half-graben structure, which dips down to the east or down to the west toward the northern symmetric graben with a broad flatter basin center. In contrast to the 23–13 Ma tectonic quiescent phase that was proposed in several publications, we conclude that rifting activity, with ongoing faulting and subsidence, was continuous from at least the late Oligocene through the Miocene and Pliocene and possibly to the Quaternary-present. The new comprehensive geometry and newly proposed temporal continuity of the rifting activity fit with a new model for Terror Rift emplacement in which an early east-west extensional episode successively evolved into dextral transtensional motion or oblique rifting at ~26 Ma (Granot & Dyment, 2018). The results of this work will also influence broader studies on the evolution of the development of the ice sheet and coastal glacial systems across the TAM during the Cenozoic. Improved knowledge of the tectonic framework will help to define the boundary conditions for glacioisostatic modeling and paleosea floor depth reconstructions, which are crucial for estimating the sensitivity of the ice sheet to past and future climate changes.

Data Availability Statement

The seismic stratigraphic interpretation for much of Ross Sea has been provided to the US Antarctic Program Data Center at <http://www.usap-dc.org/view/dataset/601098>. Information about the grids is given at: <https://www.usap-dc.org/readme/601098>.

References

- Allen P. A., & Allen J. R. (Eds.), (1990). *Basin analysis. Principles & applications*. Oxford, London, Edinburgh, Boston, Melbourne: Blackwell Scientific.
- Anderson, J. B., & Bartek, L. R. (1992). Cenozoic glacial history of the Ross Sea revealed by intermediate resolution seismic reflection data combined with drill site information. In J. P. Kennett, & D. Warnke (Eds.), *The Antarctic paleoenvironment: A perspective on global change*, Antarctic Research series (Vol. 56, pp. 231–263). Washington, DC: American Geophysical Union.
- Barrett, P. J. (1986). Antarctic Cenozoic history from the MSSTS-1 drillhole, McMurdo Sound, Antarctica. *New Zealand Department of Scientific and Industrial Research Bulletin*, 237, 174.

Acknowledgment

Funded by PNRA (Programma Nazionale di Ricerca in Antartide) in the framework of Projects Vild and Rossmap. The study was supported also by NSF funding NSF-OCE PLR 1341585 to Sorlien and Luyendyk. We acknowledge the SCAR Antarctic Seismic Data Library System for Cooperative Research (<https://sdls.ogs.trieste.it/>; Childs et al., 1994) for the MCS data availability and Terry Wilson and Stuart Henrys for the use of NBP0401 profiles through the SDLS. We acknowledge IHS Markit for the academic license of Kingdom Suite software, GeoMapApp (www.geomapapp.org) and the Istituto Nazionale di Oceanografia e di Geofisica Sperimentale—OGS—and the UC Santa Barbara—UCSB—for logistic, instruments and utilities supply. We want to thank Doug Wilson for scientific discussion and contribution. Furthermore, we want to acknowledge Rossmap participants, Fred Davey, Roi Granot, Phil Bart, Lou Bartek, Gualtiero Bohm. Our acknowledgment is also for Roi Granot, Christine Siddoway and Florence Colleoni for significant help. We thank the two anonymous reviewers and Dennis Harry whose comments and suggestions helped to improve this manuscript.

- Barrett, P. J. (1989). Antarctic Cenozoic history from the CIROS-1 drillhole, McMurdo Sound, Antarctica. *New Zealand Department of Scientific and Industrial Research Bulletin*, 245, 254.
- Barrett, P. J., & Scientific Staff (1985). Plio-Pleistocene glacial sequence cored at CIROS 2 Ferrar Fjord, western McMurdo Sound. *Victoria University Antarctic Research Expedition Science and Logistics Reports*, 29(6, 2), 8–19.
- Bart, P. J. (2004). West-directed flow of the West Antarctic ice sheet across Eastern Basin, Ross Sea during the quaternary. *Earth and Planetary Science Letters*, 228, 425–438. <https://doi.org/10.1016/j.epsl.2004.10.014>
- Bartek, L. R., Henrys, S. A., Anderson, J. B., & Barrett, P. J. (1996). Seismic stratigraphy of McMurdo Sound, Antarctica: Implications for glacially influenced early Cenozoic eustatic change?. *Marine Geology*, 130(1–2), 79–98 [https://doi.org/10.1016/0025-3227\(95\)00121-2](https://doi.org/10.1016/0025-3227(95)00121-2)
- Blackman, D. K., Von Herzen, R. P., & Lawver, L. A. (1987). Heat flow and tectonics in the Western Ross Sea, Antarctica. In A. K. Cooper, & F. J. Davey (Eds.), *The Antarctic margin: Geology and Geophysics of the Western Ross Sea, Earth science series* (pp. 179–189). Houston, TX: Circum-Pacific Council of Energy and Mineral Resources.
- Blocher, W. (2017). *Fault geometry and kinematics within the Terror rift, Antarctica*. Ohio State University. Retrieved from <https://etd.ohiolink.edu>
- Brancolini, G., Busetti, M., Marchetti, A., De Santis, L., Zanolla, C., Cooper, A. K., et al. (1995a). Seismic stratigraphic atlas of the Ross Sea, Antarctica. In A. K. Cooper, P. F. Barker, G. Brancolini (Eds.), *Geology and seismic stratigraphy of the Antarctic margin, Antarctic Research series* (Vol. 68, pp. 271–286). Washington, DC: American Geophysical Union.
- Brancolini, G., Cooper, A. K., & Coren, F. (1995b). Seismic facies and glacial history in the Western Ross Sea (Antarctica). In A. K. Cooper, P. F. Barker, & G. Brancolini (Eds.), *Geology and seismic stratigraphy of the Antarctic margin, Antarctic Research series* (Vol. 68, pp. 209–233). Washington, DC: American Geophysical Union.
- Brankman, C. M., & Shaw, J. H. (2009). Structural geometry and slip of the Palos Verdes fault, southern California: Implications for earthquake hazards. *Bulletin of the Seismological Society of America*, 99(3), 1730–1745. <https://doi.org/10.1785/0120080303>
- Brazell, S. J. (2017). *Seismic record of West Antarctic ice sheet dynamics during the late Oligocene to early Miocene in the Eastern Basin, Ross Sea*. (Doctoral dissertation). Department of Geological Sciences, University of North Carolina at Chapel Hill.
- Cande, S. C., & Stock, J. M. (2006). Constraints on the timing of extension in the Northern Basin, Ross Sea, in Antarctica. In D. K. Futterer, D. Damaske, G. Kleinschmidt, H. Miller, & F. Tessensohn (Eds.), *Contributions to global Earth sciences* (pp. 319–326). New York, NY: Springer.
- Cande, S. C., Stock, J. M., Müller, D., & Ishihara, T. (2000). Cenozoic Motion between East and West Antarctica. *Nature*, 404, 145–150. <https://doi.org/10.1038/35004501>
- Cape Roberts Science Team (1998). Initial report on CRP-1, Cape Roberts Project. *Terra Antarctica*, 5(5), 1–187.
- Cape Roberts Science Team (1999). Studies from the Cape Roberts Project, Ross Sea, Antarctica, initial report on CRP-2/2A. *Terra Antarctica*, 6, 1–173.
- Cape Roberts Science Team (2000). Studies from the Cape Roberts Project, Ross Sea, Antarctica, initial report on CRP-3/3A. *Terra Antarctica*, 7, 1–209.
- Child, J. R., Sliter, R. W., & Cooper, A. K. (1994). A progress report on the Antarctic seismic data library system for cooperative research (SDLS). *Terra Antarctica*, 2, 243–246.
- Cochrane, G. R., Cooper, A. K., Childs, J. R., & Hart, P. E. (1992). USGS seismic refraction surveys in the Ross Sea, 1984–1990. *U.S. Geological Survey*, 92–556, 17.
- Cohen, K. M., Finney, S. C., Gibbard, P. L., & Fan, J.-X. (2013). The ICS International Chronostratigraphic Chart. *Episodes*, 36, 199–204.
- Cooper, A. K., Davey, F. J., & Behrendt, J. C. (1987a). Seismic stratigraphy and structure of the Victoria Land basin, Western Ross Sea, Antarctica. In A. K. Cooper, & F. J. Davey (Eds.), *The Antarctic continental margin, Geology and Geophysics of the Western Ross Sea*. Circum-Pacific Council for Energy and mineral resources (pp. 27–76). Houston, TX: Earth Science Series.
- Cooper, A. K., Davey, F. J., & Behrendt, J. C. (1987b). Structure of extensionally rifted crust beneath the Western Ross Sea and Iselin Bank, Antarctica, from Sonobuoy seismic data. In A. K. Cooper, & F. J. Davey (Eds.), *The Antarctic continental margin, geology and geophysics of the Western Ross Sea*. Circum-Pacific council for energy and mineral resources (pp. 93–118). Houston, TX: Earth Science Series.
- Davey, F. J., Bennett, D. J., & Houtz, R. E. (1982). Sedimentary basins of the Ross Sea, Antarctica. *Journal of Geology and Geophysics*, 25(2), 245–255. <https://doi.org/10.1080/00288306.1982.10421413>
- Davey, F. J., & Brancolini, G. (1995). The Late Mesozoic and Cenozoic structural setting of the Ross Sea region. In A. K. Cooper, P. F. Barker, & G. Brancolini (Eds.), *Geology and seismic stratigraphy of the Antarctic margin, Antarctic Research series* (pp. 167–182). Washington, DC: American Geophysical Union.
- Davey, F. J., Brancolini, G., Hamilton, R. J., Henrys, S., & Sorlien, C. C. (2000). A revised correlation of the seismic stratigraphy at the Cape Roberts drill sites with the seismic stratigraphy of the Victoria Land Basin, Antarctica. *Terra Antarctica*, 7(3), 215–220.
- Davey, F. J., Cande, S. C., & Stock, J. M. (2006). Extension in the western Ross Sea region-links between Adare Basin and Victoria Land Basin. *Geophysical Research Letters*, 33, L20315. <https://doi.org/10.1029/2006GL027383>
- Davey, F. J., & De Santis, L. (2006). A multi-phase rifting model for the Victoria Land Basin, western Ross Sea, in Antarctica: Contributions to Global Earth Sciences. In D. K. Futterer, D. Damaske, G. Kleinschmidt, & H. M. F. Tessensohn (Eds.), *Antarctica: Contributions to global earth Sciences*. (pp. 303–308). Berlin Heidelberg New York: Springer-Verlag.
- Davey, F. J., Granot, R., Cande, S. C., Stock, J. M., Selvans, M., & Ferraccioli, F. (2016). Synchronous Oceanic Spreading and Continental Rifting in West Antarctica. *Geophysical Research Letters*, 43(12), 6162–6169. <https://doi.org/10.1002/2016GL069087>
- Della Vedova, B., Gantar, C., & Zanolla, C. (1994). Crustal Structure in the Ross Sea Area, Antarctica. *Terra Antarctica*, 1, 121–122.
- Della Vedova, B., Pellis, G., & Lawver, L. A. (1992). Heat flow and active tectonics of the western Ross Sea. In Y. Yoshida, K. Kaminuma, & K. Shiraishi (Eds.), *Recent Progress in Antarctic Earth Science, Proceedings of the Sixth International Symposium on Antarctic Earth Science*. (pp. 627–637). Saitama, Japan.
- Dix, C. H. (1995). Seismic velocities from surface measurements. *Geophysics*, 20(1), 68–86. <https://doi.org/10.1190/1.1438126>
- Doglioni, C., D'Agostino, N., & Mariotti, G. (1998). Normal faulting vs regional subsidence and sedimentation rate. *Marine and Petroleum Geology*, 15, 737–750.
- Ferraccioli, F., Armadillo, E., Zunino, A., Bozzo, E., Rocchi, S., & Armienti, P. (2009). Magmatic and tectonic patterns over the Northern Victoria Land sector of the Transantarctic Mountains from new aeromagnetic imaging. *Tectonophysics*, 478(1–2), 43–61. <https://doi.org/10.1016/j.tecto.2008.11.028>
- Fielding, R. C. (2018). Stratigraphic architecture of the Cenozoic succession in the McMurdo Sound region, Antarctica: An archive of polar palaeoenvironmental change in a failed rift setting. *Sedimentology*, 65, 1–61. <https://doi.org/10.1111/sed.12413>
- Fielding, C. R., Henrys, S. A., & Wilson, T. J. (2006). Rift history of the western Victoria Land Basin: A New perspective based on integration of cores with seismic reflection data. In D. K. Futterer, D. Damaske, G. Kleinschmidt, H. Miller, & F. Tessensohn (Eds.), *Antarctica: Contributions to global Earth sciences*. (pp. 309–318). Berlin: Springer-Verlag.

- Fielding, C. R., & Thomson, M. R. A. (Eds.), (1999). *Studies from the Cape Roberts Project Ross Sea, Antarctica Initial Report on CRP-2/2A*. (Vol. 6, pp. 1–173). Terra Antarctica.
- Fielding, C. R., Whittaker, J., Henrys, S. A., Wilson, T. J., & Naish, T. R. (2008). Seismic facies and stratigraphy of the Cenozoic succession in McMurdo Sound, Antarctica: Implications for tectonic, climatic and glacial history. *Palaeogeography, Palaeoclimatology, Palaeoecology*, 260, 8–29. <https://doi.org/10.3133/of2007-1047.srp090>
- Fitzgerald, P. G., & Baldwin, S. L. (1997). Detachment fault model for the evolution of the Ross Embayment. In C. A. Ricci (Ed.), *The Antarctic region: Geological evolution and processes*. (pp. 555–564). Siena: Terra Antarctica Publications.
- Fossen, H., Odinsen, T., Færseth, R. B., Roy, H., & Gabrielsen, R. H. (2000). Detachments and low-angle faults in the northern North Sea rift system. *Geological Society, London, Special Publications*, 167, 105–131. <https://doi.org/10.1144/GSL.SP.2000.167.01.06>
- Giggenbach, W. F., Kyle, P. R., & Lyon, G. L. (1973). Present volcanic activity on Mount Erebus, Ross Island. Antarctica. *Geology*, 1, 135–136. [https://doi.org/10.1130/0091-7613\(1973\)1<135:PVAOME>2.0.CO;2](https://doi.org/10.1130/0091-7613(1973)1<135:PVAOME>2.0.CO;2)
- Granot, R., Cande, S. C., Stock, J. M., & Damaske, D. (2013). Revised Eocene-Oligocene kinematics for the West Antarctic rift system. *Geophysical Research Letters*, 40, 279–284. <https://doi.org/10.1029/2012GL054181>
- Granot, R., Cande, S. C., Stock, J. M., Davey, F. J., & Clayton, R. W. (2010). Postspreading rifting in the Adare Basin, Antarctica: Regional tectonic consequences. *Geochemistry, Geophysics, Geosystems*, 11, Q08005. <https://doi.org/10.1029/2010GC003105>
- Granot, R., & Dymit, J. (2018). Late Cenozoic unification of East and West Antarctica. *Nature Communications*, 9, 3189. <https://doi.org/10.1038/s41467-018-05270-w>
- Hall, J., Wilson, T., & Henrys, S. (2007). Structure of the central Terror rift, western Ross Sea, Antarctica. U.S. Geological Survey and The National Academies. <https://doi.org/10.3133/of2007-1047.srp108>
- Hamilton, R., Sorlien, C. C., Luyendyk, B. P., & Bartek, L. R. (2001). Cenozoic tectonics of the Cape Roberts rift basin and Transantarctic Mountains front, southwestern Ross Sea, Antarctica. *Tectonics*, 20, 325–342. <https://doi.org/10.1029/2000TC001218>
- Hampel, A., Hetzel, R., & Maniatis, G. (2010). Response of faults to climate-driven changes in ice and water volumes on Earth's surface. *Philosophical Transaction of the Royal Society*, 368, 2501–2517. <https://doi.org/10.1098/rsta.2010.0031>
- Haq, B. U., Hardenbol, J., & Vail, P. R. (1987). Chronology of fluctuating sea levels since the Triassic. *Science*, 235, 1156–1167. <https://doi.org/10.1126/science.235.4793.1156>
- Harwood, D. M. (1989). Siliceous microfossils. In P. J. Barrett (Ed.), *Antarctic Cenozoic history from the CIROS-1 drillhole, McMurdo Sound*. (Vol. 245, pp. 67–97). DSIR Bulletin.
- Hayes, D. E., & Frakes, L. A. (1975). *Initial reports of the Deep Sea drilling Project*, 28. Washington U.S. Government Printing Office.
- Henrys, S. A., Wilson, T., Whittaker, J. M., Fielding, C., Hall, J., & Naish, T. (2007). Tectonic history of mid-Miocene to present southern Victoria Land Basin, inferred from seismic stratigraphy in McMurdo Sound, Antarctica. In A. K. Cooper et al. (Eds.), *Antarctica: A Keystone in a Changing World—Online Proceedings of the 10th International Symposium on Antarctic Earth Sciences, US Geological Survey Open-File Report 2007-1047*. <https://doi.org/10.3133/of2007-1047.srp049>
- Horgan, H., Naish, T., Bannister, S., Balfour, N., & Wilson, G. (2005). Seismic stratigraphy of the Plio-Pleistocene Ross Island flexural moat-fill: A prognosis for ANDRILL Program drilling beneath McMurdo-Ross Ice Shelf. *Global and Planetary Change*, 45(1–3), 83–97. <https://doi.org/10.1016/j.gloplacha.2004.09.014>
- Houtz, R. E., & Davey, F. J. (1973). Seismic profiler and sonobuoy measurements in the Ross Sea, Antarctica. *Journal of Geophysical Research*, 78, 3448–3468. <https://doi.org/10.1029/JB078i017p03448>
- Jordan, T. A., Riley, T. R., & Siddoway, C. S. (2020). The geological history and evolution of West Antarctica. *Nature Review Earth & Environment*, 1, 117–133. <https://doi.org/10.1038/s43017-019-0013-6>
- Kulhanek, D. K., Levy, R. H., Clowes, C. D., Prebble, J. G., Rodelli, D., Jovane, et al. (2019). Revised chronostratigraphy of DSDP Site 270 and late Oligocene to early Miocene paleoecology of the Ross Sea sector of Antarctica. *Global and Planetary Change*, 178, 46–64. <https://doi.org/10.1016/j.gloplacha.2019.04.002>
- Kyle, P. R. (1990). McMurdo Volcanic Group—Western Ross Embayment: Introduction. In W. E. LeMasurier, & J. W. Thomson (Eds.), *Volcanoes of the Antarctic plate and Southern oceans*, Antarctic Research series (Vol. 48). Washington, DC: American Geophysical Union.
- Kyle, P. R., Moore, J. A., & Thirlwall, M. F. (1992). Petrologic evolution of anorthoclase phonolite lavas at Mount Erebus, Ross Island, Antarctica. *Journal of Petroleum*, 33, 849–875. <https://doi.org/10.1093/petrology/33.4.849>
- Lawver, L. A., & Gahagan, L. M. (1994). Constraints on timing of extension in the Ross Sea Region. *Terra Antarctica*, 1, 545–552.
- Lowell, J. D. (1972). Spitsbergen Tertiary orogenic belt and the Spitsbergen fracture zone. *The Geological Society of America Bulletin*, 83, 3091–3102.
- Luyendyk, B. P., Cisowski, S., Smith, C. H., Richard, S. M., & Kimbrough, D. L. (1996). Paleomagnetic study of the northern Ford Ranges, western Marie Byrd Land, West Antarctica: A middle Cretaceous pole, and motion between West and East Antarctica?. *Tectonics*, 15, 122–141.
- McKay, R. M., Browne, G., Carter, L., Cowan, E., Dunbar, G., Krissek, L., et al. (2009). The stratigraphic signature of the late Cenozoic Antarctica Ice Sheets in the Ross Embayments. *Geological Society of America Bulletin*, 121, 1537–1561. <https://doi.org/10.1130/B26540.1>
- McKay, R. M., De Santis, L., & Kulhanek, D. K., & the Expedition 374 Scientists (2019). Ross Sea West Antarctic Ice Sheet History. *Proceedings of the International Ocean Discovery Program*, 374. College Station, TX: International Ocean Discovery Program. <https://doi.org/10.14379/iop.proc.374.2019>
- Mukherjee, S., & Khonsari, M. M. (2018). Inter-book normal fault-related shear heating in brittle bookshelf faults. *Marine and Petroleum Geology*, 97, 45–48.
- Naish, T., Powell, R., & Levy, R. (2007). Studies from the ANDRILL McMurdo Ice Shelf Project, Antarctica: Initial science report on AND-1B. *Terra Antarctica*, 14, 328.
- Naish, T., Powell, R., Levy, R., Wilson, G., Scherer, R., Talarico, F., et al. (2009). Obliquity-paced Pliocene West Antarctic Ice Sheet oscillations. *Nature*, 458, 322–328. <https://doi.org/10.1038/nature07867>
- Olivetti, V., Rossetti, F., Balestrieri, M. L., Pace, D., Cornamusini, G., & Talarico, F. (2018). Variability in uplift, exhumation and crustal deformation along the Transantarctic Mountains front in southern Victoria Land, Antarctica. *Tectonophysics*, 745, 229–244. <https://doi.org/10.1016/j.tecto.2018.08.017>
- Pekar, S. F., Speece, M. A., Wilson, G. S., Sunwall, D. S., & Tinto, K. J. (2013). *The Offshore New Harbour Project: Deciphering the Middle Miocene through Late Eocene seismic stratigraphy of Offshore New Harbour, western Ross Sea, Antarctica*. (Vol. 381, pp. 199–213). Geological Society of London Special Publications. <https://doi.org/10.1144/SP381.2>
- Ramsay, J. G., & Huber, M. L. (1987). *The techniques of modern structural geology*. (p.700). Orlando, FL: Academia Press.
- Rilling, S. E., Mukasa, S. B., Wilson, T. J., & Lawver, L. A. (2007). ⁴⁰Ar-³⁹Ar Age constraints on volcanism and tectonism in the Terror rift of the Ross Sea, Antarctica. U.S. Geological Survey and The National Academies. <https://doi.org/10.3133/of2007-1047.srp092>

- Rossetti, F., Storti, F., Busetti, M., Lisker, F., Di Vincenzo, G., Läufer, A., et al. (2006). Eocene initiation of Ross Sea dextral faulting and implications for East Antarctic neotectonics. *Journal of the Geological Society*, 163, 119–126. <https://doi.org/10.1144/0016-764905-005>
- Rowe, C. A., Aster, R. C., Kyle, P. R., Dibble, R. R., & Schlue, J. W. (2000). Seismic and acoustic observations at Mount Erebus Volcano, Ross Island, Antarctica, 1994–1998. *Journal of Volcanology and Geothermal Research*, 101, 105–128. [https://doi.org/10.1016/S0377-0273\(00\)00170-0](https://doi.org/10.1016/S0377-0273(00)00170-0)
- Ryan, W. B. F., Carbotte, S. M., Coplan, J. O., O'Hara, S., Melkonian, A., Arko, R., et al. (2009). Global Multi-Resolution Topography synthesis. *Geochemistry, Geophysics, Geosystems*, 10, Q03014. <https://doi.org/10.1029/2008GC002332>
- Sagnotti, L., Florindo, F., Verosub, K. L., Wilson, G. S., & Roberts, A. P. (1998). Environmental magnetic record of Antarctic palaeoclimate from Eocene/Oligocene glaciomarine sediments, Victoria Land Basin. *Geophysical Journal International*, 134(3), 653–662. <https://doi.org/10.1046/j.1365-246x.1998.00559.x>
- Salvini, F., Brancolini, G., Busetti, M., Storti, F., Mazzarini, F., & Coren, F. (1997). Cenozoic geodynamics of the Ross Sea Region, Antarctica: Crustal extension, intraplate strike-slip faulting and tectonic inheritance. *Journal of Geophysical Research*, 102(B11), 24669–24696. <https://doi.org/10.1029/97JB01643>
- Salvini, F., & Storti, F. (1999). Cenozoic tectonic lineaments of the Terra Nova Bay region, Ross Embayment, Antarctica. *Global and Planetary Change*, 23(1), 129–144. [https://doi.org/10.1016/S0921-8181\(99\)00054-5](https://doi.org/10.1016/S0921-8181(99)00054-5)
- Sato, S., Asakura, N., Saki, T., Oikawa, N., & Kaneda, Y. (1984). Preliminary results of geological and geophysical surveys in the Ross Sea and in the Dumont d'Urville Sea, off Antarctica. *Memoirs of National Institute of Polar Research, Special Issue*, 33, 66–92.
- Sauli, C., Busetti, M., De Santis, L., & Wardell, N. (2014). Late Neogene geomorphological and glacial reconstruction of the northern Victoria Land coast, western Ross Sea (Antarctica). *Marine Geology*, 355, 297–309. <https://doi.org/10.1016/j.margeo.2014.06.008>
- Savage, M. L., & Ciesielsky, P. F. (1983). Revised History of Glacial Sedimentation in the Ross Sea Region. *Proceedings of the Fourth International Symposium on Antarctic Earth Sciences*. (pp. 555–559). South Australia: University of Adelaide.
- Siddoway, C., Baldwin, S., Fitzgerald, P., Fanning, C., & Luyendyk, B. (2004). Ross Sea Mylonites and the timing of intracontinental extension within the West Antarctic rift system. *Geology*, 32, 57–60. <https://doi.org/10.1130/G20005.1>
- ANDRILL Science Team, 2010. An integrated age model for the ANDRILL-2A drill core. In K. Kontar, D. M. Harwood, F. Florindo, S. Fischbein (Compilers), *ANDRILL southern McMurdo Sound Project science integration workshop*, (Vol. 16, pp 12–13). Erice, Italy: ANDRILL Contribution, 6–11th April, 2010.
- Sorlien, C. C., Bennett, J. T., Cormier, M. H., Campbell, B. A., Nicholson, C., & Bauer, R. L. (2015). Late Miocene–Quaternary fault evolution and interaction in the southern California Inner Continental Borderland. *Geosphere*, 11(4), 1111–1132. <https://doi.org/10.1130/GES0118.1>
- Sorlien, C. C., Sauli, C., De Santis, L., Luyendyk, B. P., Wardell, N., Davis, S. M., et al. (2016). *Seismic stratigraphic interpretations suggest that sectors of the central and western Ross Sea were near and above sea level during earliest Oligocene time*. San Francisco, CA: Paper Presented at AGU Fall Meeting.
- Sorlien, C., Sauli, C., De Santis, L., Luyendyk, B. P., Wardell, N., Davis, S. M., et al. (2019). *Ross Sea unconformities digital grids in depth and two-way time*. U.S. Antarctic Program (USAP) Data Center. <https://doi.org/10.15784/601098>
- Sorlien, C. C., Seeber, L., Broderick, K. G., Luyendyk, B. P., Fisher, M. A., Sliter, R. W., & Normark, W. R. (2013). The Palos Verdes Anticlinorium along the Los Angeles, California coast: Implications for underlying thrust faulting. *Geochemistry, Geophysics, Geosystems*, 14, 1866–1890. <https://doi.org/10.1002/ggge.20112>
- Steckler, M. S., & Watts, A. B. (1978). Subsidence of the Atlantic-type continental margin off New York. *Earth and Planetary Science Letters*, 41, 1–13. [https://doi.org/10.1016/0012-821X\(78\)90036-5](https://doi.org/10.1016/0012-821X(78)90036-5)
- Storti, F., Balestrieri, M. L., Balsamo, F., & Rossetti, F. (2008). Structural and thermochronological constraints to the evolution of the West Antarctic Rift System in central Victoria Land. *Tectonics*, 27(4), 1–21, TC4012. <https://doi.org/10.1029/2006TC002066>
- Sylvester, A. G. (1988). Strike-slip faults. *Geological Society of America Bulletin*, 100, 1666–1703. [https://doi.org/10.1130/0016-7606\(1988\)100<1666:SSF>2.3.CO;2](https://doi.org/10.1130/0016-7606(1988)100<1666:SSF>2.3.CO;2)
- Tankersley, M., Siddoway, C. S., Tinto, K. J., Wilner, J. A., & Bell, R. E. (2018). *Aerogeophysical analysis of Crustal structures under the Ross ice shelf*. San Francisco, CA: Paper presented at AGU Fall Meeting.
- Tinto, K. J., Padman, L., Siddoway, C. S., Springer, S. R., Fricker, H. A., Das, I., et al. (2019). Ross ice shelf response to climate driven by the tectonic imprint on seafloor bathymetry. *Nature Geoscience*, 12(6), 441–449. <https://doi.org/10.1038/s41561-019-0370-2>
- Watts, A. B., & Ryan, W. B. F. (1976). Flexure of the lithosphere and continental margin basins. *Tectonophysics*, 36, 25–44. [https://doi.org/10.1016/0040-1951\(76\)90004-4](https://doi.org/10.1016/0040-1951(76)90004-4)
- Wenman, P., Harry, D. L., & Jha, S. (2020). Tectonic and stratigraphic evolution of the Victoria Land Basin and Ross Island Flexural Moat, West Antarctica. *Geochemistry, Geophysics, Geosystems*, 21, e2019GC008568. <https://doi.org/10.1029/2019GC008568>
- Whittaker, J. (2005). *Cenozoic structural and stratigraphic history of McMurdo Sound, Antarctica*. (Master's thesis). Wellington, New Zealand: Retrieved from Victoria University of Wellington.
- Wilson, T. J. (1995). Cenozoic transtension along the Transantarctic Mountains–West Antarctic rift boundary, Southern Victoria Land, Antarctica. *Tectonics*, 14, 531–545. <https://doi.org/10.1029/94TC02441>
- Wilson, G., Levy, R., Naish, T., Powell, R., Florindo, F., Ohneiser, C., et al. (2012). Neogene tectonic and climatic evolution of the Western Ross Sea, Antarctica—Chronology of events from the AND-1B drill hole. *Global and Planetary Change*, 96–97, 189–203. <https://doi.org/10.1016/j.gloplacha.2012.05.019>
- Wilson, D. S., & Luyendyk, B. P. (2009). West Antarctic paleotopography estimated at the Eocene–Oligocene climate transition. *Geophysical Research Letter*, 36, L16302. <https://doi.org/10.1029/2009GL039297>
- Wilson, G. S., Roberts, A. P., Verosub, K. L., Florindo, F., & Sagnotti, L. (1998). Magnetobiostratigraphic chronology of the Eocene Oligocene transition in the CIROS-1core, Victoria Land Margin, Antarctica: Implications for Antarctic glacial history. *Geological Society of America Bulletin*, 110, 35–47.
- Winter, D. M., & Harwood, D. M. (1997). Integrated diatom biostratigraphy of late Neogene drillholes in southern Victoria Land and correlation to Southern Ocean records. In C. A. Ricci (Ed.), *The Antarctic Region: geological evolution and processes: Proceedings of the VII International Symposium on Antarctic Earth Sciences*, Siena, Italy. (Vol. 7, pp. 985–992). Terra Antartica.
- Withjack, M. O., Islam, Q. T., & La Pointe, P. R. (1995). Normal faults and their hanging-wall deformation: An experimental study. *American Association of Petroleum Geologists Bulletin*, 79, 1–18.
- Xiao, H., & Suppe, J. (1992). Origin of rollover. *American Association of Petroleum Geologists Bulletin*, 76, 509–525.